Decreased microglial Wnt/β-catenin signalling drives microglial pro-inflammatory activation in the developing brain

Juliette van Steenwinckel, Anne-Laure Schang, Michelle L Krishnan, Vincent Degos, Andrée Delahaye-Duriez, Cindy Bokobza, Zsolt Csaba, Franck Verdonk, Amélie Montané, Stéphanie Sigaut, et al.

Decreased microglial Wnt/β-catenin signalling drives microglial pro-inflammatory activation in the developing brain

Running title: Regulation of microglial activation by Wnt

Juliette Van Steenwinckel [1,2], Anne-Laure Schang [1-3], Michelle L Krishnan [4], Vincent Degos [1,2,5], Andrée Delahaye-Duriez [1,6], Cindy Bokobza[1-2], Zsolt Csaba[1,2], Franck Verdonk [7,8] Amélie Montané[1,2], Stéphanie Sigaut [1,2], Olivier Hennebert [1,2,9], Sophie Lebon [1,2], Leslie Schwendimann [1,2], Tifenn Le Charpentier [1,2], Rahma Hassan-Abdi [1,2], Gareth Ball [4], Paul Aljabar [4], Alka Saxena [9], Rebecca K Holloway [11], Walter Birchmeier [12], Olivier Baud[1,2], David Rowitch [13], Veronique Miron [11], Fabrice Chretien [6-7,14], Claire Leconte [15], Valérie C Besson[15], Enrico G Petretto [16], A David Edwards [4], Henrik Hagberg [4,17], Nadia Soussi-Yanicostas [1-2], Bobbi Fleiss [1,2,4,18]* & Pierre Gressens [1,2,4]*

* Equal contribution and to whom correspondence can be addressed (details below)

[1] Université de Paris, NeuroDiderot, Inserm, F-75019 Paris, France

[2] PremUP, F-75006 Paris, France

[3] UMR CNRS 8638-Chimie Toxicologie Analytique et Cellulaire, Université Paris Descartes, Sorbonne Paris Cité, Faculté de Pharmacie de Paris, 4 Avenue de l'Observatoire, F-75006 Paris, France.

[4] Centre for the Developing Brain, Division of Imaging Sciences and Biomedical Engineering, King's College London, King's Health Partners, St. Thomas' Hospital, London, SE1 7EH, United Kingdom

[5] Department of Anesthesia and Intensive Care, Pitié Salpétrière Hospital, F-75013 Paris France

[6] UFR de Santé, Médecine et Biologie Humaine, Université Paris 13, Sorbonne Paris Cité, F-93000 Bobigny, France

[7] Infection and Epidemiology Department, Human Histopathology and Animal Models Unit, Institut Pasteur, F-75015 Paris, France

[8] Paris Descartes University, Sorbonne Paris Cité, F-75006 Paris, France

[9] Conservatoire national des arts et métiers, F-75003 Paris, France

[10] Genomics Core Facility, NIHR Biomedical Research Centre, Guy's and St Thomas' NHS Foundation Trust, London, SE1 9RT, United Kingdom

[11] MRC Centre for Reproductive Health, The Queen's Medical Research Institute, The University of Edinburgh, Edinburgh, EH16 4TJ, United Kingdom
[12] Cancer Research Program, Max Delbrueck Center for Molecular Medicine in the Helmholtz Society, Berlin-Buch, Germany
[13] Department of Paediatrics, University of Cambridge, Cambridge, CB2 0QQ, United Kingdom
[14] Laboratoire de Neuropathologie, Centre Hospitalier Sainte Anne, F-75014 Paris, France
[15] EA4475 – Pharmacologie de la Circulation Cérébrale, Faculté de Pharmacie de Paris, Université Paris Descartes, Sorbonne Paris Cité, F-75006 Paris, France.
[16] Duke-NUS Medical School, 8 College Road 169857, Singapore
[17] Perinatal Center, Institute of Clinical Sciences and Institute of Neuroscience & Physiology, Sahlgrenska Academy, Gothenburg University, 41390 Gothenburg, Sweden
[18.] School of Health and Biomedical Sciences, RMIT University, Bundoora, 3083, VIC, Australia

Correspondence should be addressed to either:
Dr Pierre Gressens: Inserm U1141, Robert Debre Hospital, 48 Blvd Serurier, F-75019 Paris, France; Tel +33778648595; pierre.gressens@inserm.fr (lead contact)

Dr Bobbi Fleiss: RMIT University - Bundoora Campus. Plenty Rd., Bundoora, Victoria, Australia, 3083; bobbi.fleiss@rmit.edu.au

Abstract

Microglia of the developing brain have unique functional properties but how their activation states are regulated is poorly understood. Inflammatory activation of microglia in the still-developing brain of preterm born infants is associated with permanent neurological sequelae in 9 million infants every year. Investigating the regulators of microglial activation in the developing brain across models of neuroinflammation-mediated injury (mouse, zebrafish) and primary human and mouse microglia we found using analysis of genes and proteins that a reduction in Wnt/β-catenin signalling is necessary and sufficient to drive a microglial phenotype causing hypomyelination. We validated in a cohort of preterm born infants that genomic variation in the *WNT* pathway is associated with the levels of connectivity found in their brains. Using a Wnt agonist delivered by a BBB penetrant microglia-specific targeting nanocarrier we prevented in our animal model the pro-inflammatory microglial activation, white matter injury and behavioural deficits. Collectively, these data validate that the Wnt pathway regulates microglial activation, is critical in the evolution of an important form of human brain injury and is a viable therapeutic target.

Additional keywords

Neuroprotection, 3DNA, nanoparticle, neuroinflammation, neonatal encephalopathy, innate immunity.

Conflict of interest statement

The authors have declared that no conflicts of interest exist

Introduction

Neuroinflammation is a key pathological mechanism in almost all acute and degenerative diseases in both the adult and in the developing brain(Perry *et al.*, 2010; Hagberg *et al.*, 2012; Hickman *et al.*, 2018). Microglia (MG) and infiltrating macrophages (Mφ) are major contributors to neuroinflammation(Perry *et al.*, 2010). These cells are capable of acquiring numerous complex functional states dependent on the specific nature of an insult or injury, including cytotoxic responses, immune regulation, or injury resolution(Michell-Robinson *et al.*, 2015; Wolf *et al.*, 2017). Limiting the cytotoxic activation of MG/Mφ while promoting injury resolution represents a rational neuroprotective strategy(Rivest, 2009; Miron *et al.*, 2013), that requires an in-depth understanding of the molecular mechanisms controlling their phenotypes across forms of injury. Understanding of these regulatory mechanisms is increasing at an extraordinary rate for adult disorders. However, MG do not reach maturity until around the time of birth in humans, or the equivalent developmental time point of approximately postnatal day 14 in rodents(Butovsky *et al.*, 2014; Bennett *et al.*, 2016; Miyamoto *et al.*, 2016; Krasemann *et al.*, 2017). These MG, termed pre-microglia(Matcovitch-Natan *et al.*, 2016), have specialised functions in brain development(Thion *et al.*, 2018), but there is a striking paucity of knowledge on the regulators of MG phenotype that is relevant to injury/insult to the developing brain.

Preterm birth is the commonest cause of death and disability in children under 5 years of age, exceeding deaths from malaria or pneumonia(Lim *et al.*, 2012). Preterm birth, birth before 37 of 40 weeks' gestation, occurs in fifteen million infants yearly, rates are increasing in developed countries (e.g. 7% of all births in the UK; 13% in the US) and we are limited in our predictive and therapeutic options for these vulnerable infants. Up to 60% of infants born preterm will be left with persistent cognitive and neuropsychiatric deficits including autism-spectrum, attention-deficit disorders and epilepsy(Wood *et al.*, 2000; Delobel-Ayoub *et al.*, 2009). Insights into the previously poorly understood pathophysiology of preterm birth(Back *et al.*, 2005; Billiards *et al.*, 2008; Delobel-Ayoub *et al.*, 2009; Moore *et al.*, 2012; Verney *et al.*, 2012) have enabled us to design animal models of improved relevance to the constellation of injuries seen in contemporary cohort of infants, collectively called encephalopathy of the premature infant. Encephalopathy of the premature infant involves cerebral white matter injury due to oligodendrocyte maturation blockade and the most severe of injuries widespread neuronal/axonal disease, both of which are linked to the activation of MG/Mφ(Volpe, 2009b). The strongest predictor for outcomes we currently have in encephalopathy of the premature

infant is the severity of white matter / connectivity changes(Woodward *et al.*, 2006; Nosarti *et al.*, 2008; Spittle *et al.*, 2009; Nosarti *et al.*, 2014). MG/Mφ activation driving neuroinflammation in preterm born infants is often caused by exposure to maternal fetal infections or inflammation, such as chorioamnionitis, or post-natal sepsis(Hagberg and Mallard, 2005; Hagberg *et al.*, 2015). Endemic but often clinically silent maternal inflammatory events are considered the chief cause of preterm birth(Wu *et al.*, 2009). As such, exposure to inflammation is both a driver of preterm birth and of brain injury, and further highlighting its importance, increased indices of exposure to inflammation are the strongest predictor of poor neurological outcome(Hillier *et al.*, 1993; Dammann and Leviton, 2004; Wu *et al.*, 2009).

The Wnt (wingless-type MMTV [mouse mammary tumour virus] integration site) pathways are divided into the canonical Wnt/β-catenin, the non-canonical Wnt/planar cell polarity (PCP) pathways and the Wnt/calcium pathway. The Wnt pathways have well studied critical roles in the early developmental events of body axis patterning, and brain cell fate specification, proliferation and migration(Sokol, 2015). Aberrant regulation of canonical WNT/β-catenin signalling is strongly implicated in the onset and progression of numerous cancers(Zhan *et al.*, 2017). In development, the canonical Wnt pathway has been described as playing a repressive role in the maturation of oligodendrocytes(Shimizu *et al.*, 2005; Feigenson *et al.*, 2009; Feigenson *et al.*, 2011; Yuen *et al.*, 2014). However our knowledge has increased and we appreciate that elaborate spatial and temporal regulation of Wnt signalling nudges oligodendrocytes through multiple stage of maturation(Zhao *et al.*, 2016) and reviewed in (Guo *et al.*, 2015). Interestingly, Wnt signalling in endothelial cells has also been shown to have important roles in the transmigration of immune cells in the context of multiple sclerosis (Shimizu *et al.*, 2016; Lengfeld *et al.*, 2017). As such, it is clear that the effects of Wnt pathway activation are highly cell and context specific. However, a key regulatory role of the Wnt pathways in the response of MG/Mφ to injury or insult has not been demonstrated, especially in the developing brain. Although, activation of the Frizzled receptors (a family of G protein-coupled receptors) with Wnt ligands has complex effects on some facets of MG activity *in vitro*(Halleskog *et al.*, 2012; Halleskog and Schulte, 2013). Experimental evidence in other cell types also supports that the Wnt/ β-catenin pathway is involved in aspects of inflammatory signalling, namely there are links between expression of the inflammatory mediator COX2 (cyclooxygenase-2) and Wnt/β-catenin in cancer(Buchanan and DuBois, 2006), and evidence that β-catenin regulates at numerous levels the cytokine/pathogen induced activation of NF-κB(Ma and Hottiger, 2016). As such, in the hunt for a regulator of immature MG activation state with a view to therapy design the Wnt pathway is an interesting and rationale candidate.

In the present study, we used our mouse model of encephalopathy of prematurity in which we clearly demonstrate a causal link between MG/Mφ activation and a myelin deficit. This mouse model of encephalopathy of prematurity recapitulates the key neuropathological findings from preterm born infants, including a myelination deficit which is the focus of this study(Haynes *et al.*, 2008; Volpe, 2009a; Verney *et al.*, 2012). Using a combination of approaches across species, including human, we reveal for the first time that inhibition of the Wnt/β-catenin pathway is necessary and sufficient to drive this MG/Mφ pro-inflammatory phenotypic transformation. We also verified the clinical relevance of the Wnt pathway to anatomical white matter structure in a cohort of human preterm born infant brain using an integrated imaging genomics analysis. Finally, we employed a novel 3DNA nanocarrier that carries cargo across the blood brain barrier (BBB) following non-invasive intraperitoneal (i.p.) administration and that then delivers cargo specifically to MG/Mφ. Using this 3DNA nanocarrier we show that preventing Wnt pathway down-regulation specifically in MG/Mφ reduces the pro-inflammatory MG/Mφ phenotype, white matter damage and long-term memory deficit in our model of encephalopathy of prematurity.

Altogether, these findings identify the Wnt/β-catenin pathway as a key regulator of MG/Mφ activation state across species and a potential target for the treatment of encephalopathy of prematurity and other neuroinflammatory conditions.

Materials and Methods

Study approval

Experimental protocols were approved by the institutional guidelines of the Institut National de la Santé et de la Recherché Scientifique (Inserm, France) (Approval 2012-15/676-0079) and then the Ethic committee and the services of the French ministry in charge of higher education and research according the directive 2010/63/EU of the European Parliament (Approval #9285-2016090611282348 and #9286-2016090617132750), and met the guidelines for the United States Public Health Service's Policy on Humane Care and Use of Laboratory Animals (NIH, Bethesda, Maryland, USA).

The EPRIME study was reviewed and approved by the National Research Ethics Service, and all infants were studied following written consent from their parents.

For human MG cell culture, all procedures had ethical approval from Agence de Biomédicine (Approval PFS12-0011). Written informed consent was received from the tissue donor.

Study design

A summary of the independent and total replicates for all experiments, described relative to the figures, is available in **Supp Table 1**.

Nomenclature of MG phenotype

We have adopted nomenclature consistent with our previous work in primary MG(Chhor *et al.*, 2013) and the work of others (Michell-Robinson *et al.*, 2015) acknowledging that this is a simplification necessary to facilitate description of the data. To simplify, we distinguished three phenotypes according to the mRNA expression levels of markers listed in brackets: Pro-inflammatory (*Nos2, Ptgs2, Cd32, Cd86* and *Tnfα*), anti-inflammatory (*Arg1, Cd206, Lgals3, Igf1, Il4 and Il10*) and immunoregulatory (*Il1rn, Il4ra, Socs3* and *Sphk1*).

Mice

Experiments were performed with male OF1 strain mice pups from adult females purchased from Charles River (L'Arbresle, France) or Transgenic (Tg) male mice born in our animal facility. See the justification below in animal model section regarding use of male mice only. Tg mice B6.129P-Cx3cr1^{tm1Litt}/J (CX3CR1-GFP) mice, B6.129-Ctnnb1^{tm2Kem}/KnwJ (β-catenin^{lfox}) mice and B6.129P2-Lyz2$^{tm1(cre)Ifo}$/J (LysM^{Cre}) mice were purchased from The Jackson Laboratory (ME, USA). CX3CR1-GFP mice express EGFP in monocytes, dendritic

cells, NK cells, and brain MG under control of the endogenous Cx3cr1 locus. Only heterozygous ($Cx3cr1^{GFP/+}$ and β-$catenin^{\Delta/+}$) mice were used in this study. $Cx3cr1^{GFP/+}$ are obtained by crossing $Cx3cr1^{GFP/GFP}$ with C57bl6J (WT) mice. $LysM^{Cre}$ mice are useful for Cre-lox studies of the myeloid cell lineage. Here, we used it to analyse β-catenin deficit in the brain MG by crossing β-$catenin^{flox}$ with $LysM^{Cre}$ mice. Control mice were obtained by crossing β-$catenin^{flox}$ with C57bl6J (WT) mice.

Transgenic fish lines and fish maintenance

Tg (pu1::Gal4-UAS-TagRFP)(Sieger *et al.*, 2012) fish were kept at 26.5 °C in a 14 hour light/10 hour dark cycle. Embryos were raised at 28.5 °C in E3-solution until 120 hpf for analyses.

Drugs

Mouse cytokines (IL-1β, IL-4) were purchased from R&D systems (France). LPS-EB Ultrapure was purchased from InvivoGen (France). To inhibit the Wnt/β-catenin pathway, we used XAV939 (Sigma-Aldrich, France). To activate it, we used CT99021 (Selleckchem, TX, USA), Lithium Chloride (Sigma-Aldrich, France) and L803mts (Tocris, UK). Chelerythrine was purchased from Sigma-Aldrich. To decide on the choice of modulators of Wnt, including considerations for doses and consideration of off target effects we referred to reviews on the subject and previously published works(Fancy *et al.*, 2011; Fancy *et al.*, 2014; Keats *et al.*, 2014; Tran and Zheng, 2017). The L803mts peptide and a scrambled peptide (SCR) were purchased conjugated to short oligonucleotide with disulphide bond linker from BioSynthesis (TX, USA) then hybridized to Cy3-labelled 3DNA at Genisphere (PA, USA). L803mts was chosen due to its structural properties allowing it to be conjugated to 3DNA and high tolerability have been demonstrated in mice(Kaidanovich-Beilin and Eldar-Finkelman, 2006).

Model of encephalopathy of prematurity induced by systemically driven neuroinflammation

Mice were housed under a 12-hour light-dark cycle, had access to food and water ad libitum and were weaned into same sex groups at P21. Our animal facility has no known pathogens. On P1 pups were sexed and where necessary litters were culled to 6-8 (Tg mice) or 12 (OF1 mice) pups. Assessments of injury and outcomes were made only in male animals and all pups within a litter received identical treatment to reduce any effects of differing maternal care. All experiments include pups from at least three separate litters. Allocation to PBS or IL-1β exposure was made in an cage by cage alternating manner. Systemic inflammation was induced

via intraperitoneal (i.p.) IL-1β exposure as previously described(Favrais *et al.*, 2011). Male mice only are used, as only male pups display a myelin deficit following the induction of systemic inflammation to drive neuroinflammation in this paradigm. Specifically, female mice do not have a significant loss of the MBP protein or APC positive cell number in adulthood like the male mice (P Gressens, unpublished data). This higher severity of injury in male animals is in accordance with observations of a greater burden of neurological injury in male infants following perinatal insult (Johnston and Hagberg, 2007; Twilhaar *et al.*, 2018). In brief, a 5 µl volume of phosphate-buffered saline (PBS) containing 10 µg/kg/injection of recombinant mouse IL-1β (R&D Systems, MN, USA) or of PBS alone (control) was injected i.p. in male pups twice a day (morning and evening) on days P1 to P4 and once in the morning at P5. Animal health was monitored via weight and general visual health assessment and there were no adverse events.

Morphological analysis of MG

P1 and P3 brain from Cx3Cr1-GFP mice administered PBS or IL-1β were fixed for 24 hours in 4% buffered formalin (QPath, Labonord SAS, France). Cerebral tissue was sliced along a sagittal plane on a calibrated vibratome (VT1000 S, Leica, Germany) into 100 µm thick free-floating slices. Morphological analysis of MG was assessed as previously described(Verdonk *et al.*, 2016), using spinning disk confocal system (Cell Voyager - CV1000, Japan) with a UPLSAPO 40x/NA 0.9 objective and the use of a 488-nm laser. A mosaic of more than one hundred pictures covering approximately 3.17 mm² of tissue (cortex and white matter) per brain. An automatic image analysis using a custom designed script developed with the Acapella™ image analysis software (version 2.7 - Perkin Elmer Technologies) was realize to obtain density, cell body area, number of primary, secondary and tertiary processes and the area covered by the MG processes in 2D. A complexity index was calculated to analyse the morphological modifications induced by IL-1β.

Neural tissue dissociation and CD11B+ MG or O4+ oligodendrocyte magnetic-activated cell sorting

At P1, P2, P3, P5 and P10, brains were collected for cell dissociation and CD11B+ cell separation using a magnetic coupled antibody anti-CD11B (MACS Technology), according to the manufacturer's protocol (Miltenyi Biotec, Germany) and as previously described(Schang *et al.*, 2014). In brief, mice were intracardially perfused with NaCl 0,9%. After removing the cerebellum and olfactory bulbs, the brains until were pooled (n=2-3 per sample except at at

P10, n=1) and dissociated using the Neural Tissue Dissociation Kit containing papain and the gentleMACS Octo Dissociator with Heaters. MG were enriched using the anti-CD11B (MG) MicroBeads, pelleted and conserved at -80 °C. The purity of the eluted CD11B+ fraction was verified as previously described (*15*). At P5 and P10, brains were collected for, O4+ oligodendrocytes cell separation using a magnetic coupled antibody anti-O4 (MACS Technology), according to the manufacturer's protocol (Miltenyi Biotec, Germany) and as previously described (Schang *et al.*, 2014).

RNA extraction and quantification of gene expression by real-time qPCR

Total RNA was extracted with the RNeasy mini kit according to the manufacturer's instructions (Qiagen, France). RNA quality and concentration were assessed by spectrophotometry with the NanodropTM apparatus (Thermofisher Scientific, MA, USA). Total RNA (500ng) was subjected to reverse transcription using the iScriptTM cDNA synthesis kit (Bio-Rad, France). RT-qPCR was performed in triplicate for each sample using SYBR Green Super- mix (Bio-Rad) for 40 cycles with a 2-step program (5 s of denaturation at 95°C and 10 s of annealing at 60°C). Amplification specificity was assessed with a melting curve analysis. Primers were designed using Primer3 plus software (See sequences in **Supp Table 2)**. Specific mRNA levels were calculated after normalization of the results for each sample with those for Rpl13a mRNA (reference gene). The data are presented as relative mRNA units with respect to control group (expressed as fold over control value).

Immunohistofluorescence

For frozen sections, P1 or P5 mice were intracardially perfused with 4% paraformaldehyde in 0.12M phosphate buffer solution under isoflurane anaesthesia. Brains were then post-fixed in 4% paraformaldehyde (Sigma-Aldrich, France) overnight at 4°C After 2 days in 30% sucrose 0.12M phosphate buffer solution, brains were frozen at -45°C in isopentane (Sigma-Aldrich, France) before storage at -80°C until sectioning on a cryostat (thickness14µM). Immunohistofluorescence was performed as previously described(Miron *et al.*, 2013). Slides were permeabilized and blocked for 1 hour and primary antibody was applied overnight at 4 °C in a humid chamber. To detect MG, rabbit antibody to IBA1 (Wako, 1: 500) was used. To detect proinflammatory MG we used mouse antibody to iNOS (BD Biosciences, 610329, 1:100), rat antibody to CD16/CD32 (BD Pharmingen, 553141, 1:500), rabbit antibody to COX2 (Abcam, Ab15191, 1:500). To detect anti-inflammatory MG, we used goat antibody to Arginase-1 (ARG1) (Santa Cruz Biotechnology, sc-18355, 1:50), rabbit antibody to mannose receptor

(MR) (Abcam, ab64693, 1:600). To detect MG and Mφ rat antibody to CD68 (Abcam, ab53444, 1:100) was used. Fluorescently conjugated secondary antibody to goat IgG (A21432), antibodies to rabbit IgG (A11034, A10042), antibodies to rat IgG (A21434, A11006, A21247) and antibody to mouse IgG (A21042), were applied for 2 hours at 20–25 °C in a humid chamber (1:500, Invitrogen). Following counterstaining with Hoechst, slides were coverslipped with Fluoromount-G (Southern Biotech, Cliniscience, France). Antibody isotype controls (Sigma-Aldrich) added to sections at the same final concentration as the respective primary antibodies showed little or no nonspecific staining. All manual cell counts were performed by an investigator who had been blinded to the group allocation of the sample.

In vivo treatments with XAV939, 3DNA L803mts Cy3, and Gadolinium

XAV939 (250μM, 0.5nmol/injection) or PBS/DMSO (vehicle) and 3DNA L803mts Cy3 (200ng/injection) or 3DNA SCR Cy3 (200ng/injection) (control peptide) were injected into the right ventricle of mice pups at P1 using 26-G needle linked to a 10μL Hamilton syringe mounted on a micromanipulator and coupled to a micro-injector (Harvard Apparatus, MA, USA; outflow 2 μL/min), 3DNA SCR or L803 mts Cy3 were injected 1 hour before i.p. injection of PBS or IL-1β. Three hours after PBS or IL-1β injection or 4 hours after XAV939 or vehicle injection, pups were sacrificed for CD11B-postive cell sorting. Chronic treatment with 3DNA L803mts Cy3 were performed by i.p. co-injections of PBS or IL-1β with 3DNA L803mts Cy3 (500ng/injection) or 3DNA L803mts Cy3 (500ng/injection) twice a day between P1 and P3 and once a day at P4 and P5. Effect of this treatment on myelination was analysed at P10 and behavioural tests were realized in adulthood (2-3months). To analyse uptake of 3DNA in liver and spleen, one i.p. injection of 3DNA Cy3 (500ng/injection) with PBS or IL-1β was performed and animals sacrificed 4 hours later. To analyse uptake of 3DNA in brain, animals was sacrificed 4 hours after i.c.v. injection at P1, and at the end of the i.p. treatment at P5.

Selective depletion of pro-inflammatory MG in white matter injury was performed using gadolinium chloride (GdCl3) as previously described(Miron *et al.*, 2013) with slight modifications. Briefly, PBS or Gadolinium (200nmol/injection, Sigma, France) was injected into the corpus callosum of mice pups at P1, 1 hour before i.p. injections of PBS or IL-1 β using 26-G needle linked to a 10μL Hamilton syringe mounted on a micromanipulator and coupled to a micro-injector (Harvard apparatus, outflow 2 μL/min). Effect of pro-inflammatory MG depletion on MG cell phenotype and myelination was analysed at P10.

Western Blotting

Frozen right anterior cortex from P15 mice was homogenized in RIPA Buffer (Sigma-Aldrich) containing protease inhibitors (cOmplete Tablets, Roche) in gentleMACS M tubes using a gentleMACS dissociator (Miltenyi Biotec) as per the manufacturer's instructions. Samples were centrifuged (10,000 g, 10 min, 4°C) and the pellets were stored for later use. Equal amounts of protein (25μg) as determined by BCA protein assays (Sigma-Aldrich), were diluted with Lamemli sample buffer (Biorad) containing 2-mercaptoethanol (Sigma-Aldrich) and then separated in Mini-protean TGX gels (Any kD, Biorad, 80 V for 1 h 50 min). Proteins were then electrotransferred (Trans-blot Turbi, Biorad) onto a 0.2μ nitrocellulose membrane (Trans-Blot Turbo Transfer Pack, mini, Biorad). The membrane was cut into an upper and lower portion and both were incubated in blocking solution (5% bovine serum albumin, 0.1% Tween 20 in TBS) for 1 h. The upper and lower parts were incubated respectively with mouse anti-β-actin (Sigma-Aldrich AC-74, 1:20,000) and rat anti-MBP (Millipore MAB386 1:500) overnight at 4°C in blocking solution. Blots were rinsed with 0.1% Tween 20 in TBS and incubated for 1 h with a HRP-conjugate goat anti-mouse IgG (1:2,000; sigma-Aldrich) or HRP-conjugate goat anti-rat IgG (1:10,000; Invitrogen) in blocking solution. The blots were washed three times with 0.1% Tween 20 in TBS for 5 min. Membranes were processed with the Clarity Western ECL substrate (Biorad), and the proteins of interest were investigated with Syngene PXi (Syngene) coupled to acquisition software. The immunoreactivity of four isoforms of MBP was compared with that of actin controls using NIH image J soft- ware (http://rsb.info.nih.gov/ij/).

Electron Microscopy

At P30 mice were transaortically perfused with 20 ml saline followed by 100 ml of ice-cold 2% paraformaldehyde with 2% glutaraldehyde in 0.1 M phosphate buffer, pH 7.4 (PB). Brains were post-fixed overnight in 2% paraformaldehyde at 4°C. Sagittal sections were cut on a vibratome at 70 μm thickness, post-fixed in 1% glutaraldehyde for 10 min, treated with 1% osmium for 10 min, dehydrated in an ascending series of ethanol, which included 1% uranyl-acetate in 70% ethanol. Sections were then treated with propylene oxide, equilibrated overnight in Durcupan ACM (Fluka, Buchs, Switzerland), and flat-embedded on glass slides for 48 h at 60°C. Blocks of the trunk of the corpus callosum (+0.1 mm to -0.1 mm from bregma) close to the midline were cut out from the sections and glued to blank cylinders of resin. Ultrathin sections were cut on a Reichert Ultracut S microtome and collected on pioloform-coated single-slot grids. Sections were stained with lead citrate and examined with a Hitachi HT7700 electron

microscope (Hitachi High-Technologies, Tokyo, Japan) equipped with an AMT XR-41B 4 Megapixel camera (Advanced Microscopy Techniques, Woburn, MA, USA).

The myelinated axon diameter was measured on cross-sectional axons. For each animal, images were acquired at three dorsoventral positions of three rostrocaudal levels. The thickness of the myelin sheath was assessed by determining the G ratio (axon diameter/total fiber diameter). An average of 1600 measurements of myelinated axons per animal were performed, using the Fiji version of ImageJ(Schindelin *et al.*, 2012). The axons were pooled by size according to their small (0.2–0.4 μm), medium (0.4–0.8 μm) or large (>0.8 μm) diameter. Results were compared by one-way ANOVA followed by Bonferroni's multiple comparison test, using GraphPad Prism 5.0 (Graph-Pad Software, San Diego, CA, USA). The value of $P < 0.05$ was considered statistically significant.

Behaviours - Actimetry

The horizontal (spontaneous locomotion) and vertical (rearing) activities were individually assessed in transparent activity cages (20x10x12cm) with automatic monitoring of photocell beam breaks (Imetronic, Bordeaux, France). Actimetry test was performed at ≈ 2 months (day 65), with recording every 30 minutes over 23 hours, in order to evaluate the effect of IL-1β and 3DNA treatments i.p. injections on spontaneous locomotor activity, as modified locomotor activity could lead to biased results from other behavioural tests requiring locomotion.

Behaviours - Open-field

The open-field test was performed at ≈ 2.5 months (day 80) using a square white open-field apparatus (100x100x50cm) made of plastic permeable to infrared light. Distance travelled and time spent in inactivity were recorded by a videotrack system (Viewpoint®) during the 9 minutes' test.

Behaviours - Barnes maze test

The Barnes maze test was performed at 3 months (day 90 to 105). The maze is a wet, white and circular platform (80cm diameter), brightly illuminated (400lux), raised 50cm above the floor, with 18 holes (4.5cm) equally spaced around the perimeter. A white hidden escape box (4x13x7cm), representing the target, was located under one of the holes. Prior to the test, each mouse was subjected to a habituation trial where the mouse was directly put in the escape box for 30 seconds.

Learning: the mouse was placed in the centre of the circular maze and was allowed to explore

the platform and holes for 3 minutes' maximum. The distance travelled was recorded using a Videotrack system (Viewpoint®). Latency to reach the escape box, and number of errors (number of empty holes visited) were manually noted. When the mouse found, and entered the escape box, the Videotrack recording was stopped, and the mouse remained in the escape box for an additional 10 seconds before returning to its home cage. If the mouse did not enter spontaneously, it is gently put toward the escape box, before returning to its home cage. On the first day of training, mice underwent 2 trials after the habituation trial; thereafter, 3 trials were given per day, with a 2 hours' interval.

Probe trial: on the 5th day of learning, the probe trial, with the escape box removed and lasting 90 seconds, is used to assess spatial memory performances. Time spent and distance travelled in each sextant (defined by one of the 6 parts of the maze, that includes 3 holes) were recorded. The target zone is defined as the part, which contains the target hole and two adjacent holes.

Long term trial: 15 days after learning, a new trial, with the escape box, is used to assess long-term retention memory. Escape latency and distance travelled to reach the target were recorded.

Immunohistochemistry

Brains were collected at P15 or P30 and immersed immediately after sacrifice in 4% formaldehyde for 4 days at room temperature, prior to dehydration and paraffin embedding. Section was realized using a microtome. Immunostaining was performed as previously described(Favrais *et al.*, 2011) using mouse antibody to Myelin Basic Protein (MAB382, Millipore, France 1: 500) or rabbit antibody to OLIG2 (JP18953 IBL 1:200). The intensity of the MBP immunostaining in the anterior corpus callosum and the number of OLIG2+ cells were assessed by a densitometry analysis through NIH ImageJ Software (http://imagej.nih.gov/ij/). Optical density was deduced from grey scale standardized to the photomicrograph background. Corpus callosum and/or cingulum were defined as region of interest. One measurement per section (on 40000μm^2 area) and 4 sections were analysed in each brain.

Primary mouse MG culture

Primary mixed glial cell cultures were prepared from the cortices of postnatal day 1 OF1 mice, as previously described(Chhor *et al.*, 2013). After 14 days, MG were purified and pelleted via centrifugation and re-suspended in DMEM/PS/10% FBS at a concentration of $4x10^5$ cells/mL. One or two mL/well of cell suspension was plated in 12-well (for qRT-PCR) or 6-well (for ELISA) culture plates respectively. For immunofluorescence, 250 µL of cell suspension was plated in µ-Slide 8 Well Glass Bottom (Ibidi, Biovalley, France). Post-plating, media was

replaced after 1 hour. Based on previous work from our lab(Chhor *et al.*, 2013), the day after plating, MG were exposed for 4 hours to DMEM (control) or IL-1β at 50 ng/mL, IL-4 at 20 ng/mL, diluted in DMEM. For RT-qPCR or ELISA analysis, media were removed and plates frozen at -80°C. For immunofluorescence experiments, cells were fixed at room temperature with 4% paraformaldehyde for 20 minutes.

Mixed mouse glial and OPC cultures

Cortical mixed glial cultures and purified OPC were obtained from the cortices of postnatal day 1 OF1 mice as previously described with slight modification (40). Mixed glial cells were resuspended in MEM-C, which consists of Minimal Essential Medium (MEM) supplemented with 10% FBS (Gibco), Glutamax (Gibco), and 1% PS, and plated at 2x105 cells/cm^2 onto T75 flasks for subsequent OPC purification or Ibidi 8-well chamber slides (Biovalley, France) for mixed glial culture treatment. For this purpose, mixed glial cultures were maintained in proliferation in MEM-C for 7 days, then maintained during 10-12 days in differentiation medium which consists of Dulbecco's Modified Eagle Medium (DMEM-F12) with glutamine (Gibco), N2 (Gibco) and 1% PS. Half of the wells were exposed to IL-1β (50 ng/ml) and medium was changed every 2-3 days. Alternatively, mixed glial cultures plated onto T75 flasks were maintained for 9-12 days in MEM-C and purified OPC cultures were prepared by a differential shake(McCarthy and de Vellis, 1980). OPCs were seeded onto Ibidi 8-well chamber slides at a density of 3 x 10^4 cells/cm^2 in proliferation medium which consists of MACS Neuro Medium with Neurobrew 21 (Miltenyi Biotec), Glutamax, 1% PS, FGFb and PDGFa (10 ng/ml each, Sigma-Aldrich). After 72h, differentiation was induced by FGFb and PDGFa withdrawal and by adding T3 (40 ng/ml, Sigma). Half of the wells were exposed to IL-1β (50 ng/ml). After 10-12 days (for mixed glial cultures) or 72h (for OPCs) of IL-1β, cells were fixed 20 min with 4% paraformaldehyde.

Primary human MG culture

Within 1 hour of scheduled termination (age 19 and 21 weeks of amenorrhea) brain tissues were collected from two human foetuses without any neuropathological alterations. Brain tissue (4 g) was minced and further mechanically dissociated using 1ml micropipettor in HBSS with Ca^{2+} and Mg^{2+}. Using a 70μM strainer a single cell suspension was obtained. MG/Mφ isolation were obtained using anti-CD11B (MG) microbeads (MACS Technology), according to the manufacturer's protocol (Miltenyi Biotec, Germany), as above. CD11B+ MG/Mφ were pelleted via centrifugation and re-suspended in DMEM/PS/10% FBS at a concentration of 5x10^6

cells/mL. Cells were plated in 12-well plates (1ml/well) for qRT-PCR analysis. For immunofluorescence analysis, cells were plated in µ-Slide 8 Well Glass Bottom (Ibidi, Biovalley, France). 48 hours after plating, MG were exposed for 4 hours to DMEM (control) or LPS 10 ng/mL diluted in DMEM. For RT-qPCR media were removed and plates frozen at -80°C. For immunofluorescence experiments, cells were fixed at room temperature with 4% paraformaldehyde for 20 minutes.

Immunocytofluorescence

Immunofluorescence staining was performed as previously described(Favrais *et al.*, 2011), using mouse antibody to MBP (MAB382, 1: 500; Millipore), rabbit antibody to OLIG2 (18953, 1:500 IBL-America, MN, USA), rabbit antibody to beta-catenin (E247, 1:100; Millipore), rabbit antibody to COX2 (Ab15191, 1: 400; Abcam, MA, USA) goat antibody to ARG1 (sc 18354, 1:400; Santa-Cruz, CA , USA) and IL1RA (sc 8482, 1:200, Santa-Cruz). Fluorescently conjugated secondary antibody (all Thermofisher Scientific) to mouse IgG (A21236), to rabbit IgG (A21206) and to goat IgG (A11055), were applied for 2 hours at 20–25 °C in a humid chamber (1:500, Invitrogen). Slides were coverslipped with Fluoromount-G (Southern Biotech, AL, USA). To analyse MBP labelling, MBP area was assessed as the percentage of total area above threshold using NIH ImageJ software (http://imagej.nih.gov/ij/) and was normalized to the number of Olig2-positive cells. Means were expressed as fold change over control condition.

Microarrays and data pre-processing

Gene expression quantification, including RNA extraction and quality assurance, was performed by Miltenyi Biotec on a total of 24 samples of CD11B+ cells and 20 samples of O4+ cells from the brains of mice exposed to IL-1β or PBS between P1 and P5, and sacrificed at P5 or P10. RNA was extracted and hybridised to Agilent Whole Mouse Genome Oligo Microarrays (8x60K).

Bioinformatics' gene co-expression network reconstruction

Expression data Each cell type and experimental condition was analysed separately, to investigate changes in gene expression over time in response to exposure to IL-1β or PBS. Expression values for MG (CD11B+) and oligodendrocytes (O4+) at P5 and P10 were quantile normalized.

Differential expression Probes showing high variability across time points within each cell type

were retained for further analysis (coefficient of variation above 50th centile). Probes showing differential expression between time points were identified using unpaired t-tests with Benjamini-Hochberg correction for multiple testing in the Bioconductor multitest package(Gentleman *et al.*, 2004; Schafer and Strimmer, 2005; Opgen-Rhein and Strimmer, 2007), with a false discovery rate threshold (FDR) of 10%.

Network reconstruction The co-expression network was inferred using Graphical Gaussian Models (GGM), implemented within the software package "GeneNet"(Schafer and Strimmer, 2005) in R (http://www.r-project.org/). This analysis computes partial correlations, which are a measure of conditional independence between two genes i.e. the correlation between the expression profiles of two genes after the common effects of all other genes are removed. Correction was made for multiple comparisons by setting the local false discovery rate (FDR) at ≤1%. Individual networks were reconstructed for temporally differentially expressed genes for each cell type in each experimental condition (i.e. 2 cell types x 2 conditions). The input for each GGM was a matrix of differentially expressed normalised mRNA transcript levels. The genes in each of these four co-expression networks (**Supp Figure 3E**) were functionally annotated by calculating significant enrichment of KEGG pathways using the Broad Institute MSigDB database (http://software.broadinstitute.org/gsea/msigdb/index.jsp)(Subramanian *et al.*, 2005) (**Supp Table 3)**.

Differential expression analysis was performed using the limma package (Smyth, 2004). The mouse datasets were annotated with human Ensembl gene ID using the biomaRt Bioconductor R package(Durinck *et al.*, 2009) and selecting human genes that were 'one-to-one' orthologues with mouse genes. We multiplied the adjusted P value (the –log10 of P value) by the log-transformed fold change to generate a gene-level score, which was used as a metric to 'rank' genes. GSEA (Subramanian *et al.*, 2005) was applied genome-wide to the ranked list of gene scores (reflecting both the significance and the magnitude of expression changes in IL-1β exposed MG/Mφ) to test if a group of genes (MSigDB gene sets) occupy higher (or lower) positions in the ranked gene list than what it would be expected by chance. Gene set enrichment scores and significance level of the enrichment (NES, P value, FDR) and enrichment plots were provided in the GSEA output format developed by Broad Institute of MIT and Harvard (permutations = 10,000). The GSEA was carried out accounting for the direction of IL-1β effect, i.e. considering whether a gene is upregulated or down-regulated under IL-1β exposure at P5 and P10.

Wnt/β-catenin pathway modulation in primary MG

MG transfection was realized using negative control siRNA or siRNA Axin2 (ON TARGET Plus Control Pool and ON TARGET Plus mouse Axin2-06, Thermoscientific, Dharmacon, France) at a final concentration of 30µM. Transfection was realized using the MACSfectin transfection reagent (Miltenyi biotec, Germany) in mixture of Opti-MEM and DMEM mediums for 48 hours prior to IL-1β stimulation. *Axin2* mRNA knockdown was evaluated by qRT-PCR. XAV939 and CT99021 (1µM) or PBS/DMSO (vehicle) were added to media 30 minutes before DMEM (control) or IL-1β (50 ng/ml) treatments.

PSer45 β-Catenin and β-Catenin quantification by ELISA

Quantification of PSer45 β-Catenin and β-Catenin by ELISA was realized using β-catenin pSer45 + Total PhosphoTracer ELISA Kit (ab119656, Abcam) for primary microglia or β-catenin ELISA Kit (ab1205704, Abcam) for MACSed cells. Briefly, cell lysates were obtained using lysis buffer of the kit. Total protein level was quantified using BCA method (Bicinchoninic Acid Solution and Copper (II) Sulfate Solution from Sigma, France). The ELISA was realized according to the manufacturer's instruction. Quantification of PSer45 β-Catenin is a ratio PSer45 β-Catenin/total β-Catenin. Total β-Catenin was normalized using total protein level. Total β-Catenin data are expressed as fold over control values.

Wnt/β-catenin pathway modulation in Zebrafish.

MG were visualized using pu1::Gal4-UAS::TagRFP. 72 hpf old zebrafish embryos were used for LPS microinjection (5ng/injection) in hindbrain. The Wnt/β-catenin pathway was modulated by adding LiCl (80mM), XAV939 (5µM), CT99021 (3µM) in E3-solution. Fluorescently labelled embryos were imaged using a microscope equipped with an ApoTome system (Zeiss, France) fitted with an AxioCam MRm camera (Zeiss) controlled by the Axiovision software. The thickness of the z stacks was always comprised between 2.5 and 3 µm. Fluorescence intensity was quantified by NIH ImageJ software (http://imagej.nih.gov/ij/) on grey scale images.

Preterm infant cohort

Preterm infants were recruited as part of the EPRIME (Evaluation of Magnetic Resonance (MR) Imaging to Predict Neurodevelopmental Impairment in Preterm Infants) study and were imaged at term equivalent age over a 3-year period (2010-2013) at a single centre. The EPRIME study was reviewed and approved by the National Research Ethics Service, and all infants were

studied following written consent from their parents. A total of 290 infants (gestational age 23.57 to 32.86 weeks, median 30 weeks) were scanned at term-equivalent age (38.29 to 58.28 weeks) additional cohort details available in **Supp Table 4**. Pulse oximetry, temperature, and heart rate were monitored throughout the period of image acquisition; ear protection in the form of silicone-based putty placed in the external ear (President Putty, Coltene, UK) and Mini-muffs (Natus Medical Inc., CA, USA) were used for each infant.

Image Acquisition

MRI was performed on a Philips 3-Tesla system (Best, Netherlands) using an 8-channel phased array head coil. The 3D-MPRAGE and high-resolution T2-weighted fast spin echo images were obtained before diffusion tensor imaging. Single-shot EPI DTI was acquired in the transverse plane in 32 non-collinear directions using the following parameters: repetition time (TR): 8000 ms; echo time (TE): 49 ms; slice thickness: 2 mm; field of view: 224 mm; matrix: 128 × 128 (voxel size: 1.75 × 1.75 × 2 mm^3); *b* value: 750 s/mm^2. Data were acquired with a SENSE factor of 2.

Data selection and quality control

The T2-weighted MRI anatomical scans were reviewed in order to exclude subjects with extensive brain abnormalities, major focal destructive parenchymal lesions, multiple punctate white matter lesions or white matter cysts, since these infants represent a heterogeneous minority (1-3%) with different underlying biology and clinical features to the general preterm population (Hamrick *et al.*, 2004; van Haastert *et al.*, 2011). All MR-images were assessed for the presence of image artefacts (inferior-temporal signal dropout, aliasing, field inhomogeneity, etc.) and severe motion (for head-motion criteria see below). All exclusion criteria were designed so as not to bias the study but preserve the full spectrum of clinical heterogeneity typical of a preterm born population. 290 infants had images suitable for tractography and associated genetic information.

DTI analysis was performed using FMRIB's Diffusion Toolbox (FDT v2.0). Images were registered to their non-diffusion weighted (*b*0) image and corrected for differences in spatial distortion due to eddy currents. Non-brain tissue was removed using the brain extraction tool (BET)(Smith, 2002). Diffusion tensors were calculated voxel-wise, using a simple least-squares fit of the tensor model to the diffusion data. From this, the tensor eigenvalues and FA maps were calculated.

Probabilistic tractography

Regions of interest for seeding tracts were obtained by segmentation of the brain based on a 90-node anatomical neonatal atlas(Shi *et al.*, 2011), and the resulting segmentations were registered to the diffusion space using a custom neonatal pipeline(Ball *et al.*, 2010). Tractography was performed on DTI data using a modified probabilistic tractography which estimates diffusive transfer between voxels(Robinson *et al.*, 2008), using cortico-cortical connections only. A weighted adjacency matrix of brain regions was produced for each infant: self-connections along the diagonal were removed; symmetry was enforced; and the redundant lower triangle removed. The edges of these connectivity graphs were vectorised by concatenating the rows for each individual connectivity matrix, and appending them to form a single matrix of n individuals by p edges. Each phenotype matrix was adjusted for major covariates (post-menstrual age at scan and at birth) and reduced to its first principal component.

Genome-wide genotyping

Saliva samples from 290 preterm infants with imaging data were collected using Oragene DNA OG-250 kits (DNAGenotek Inc., Kanata, Canada) and genotyped on Illumina HumanOmniExpress-24 v1.1 chip (Illumina, San Diego, CA, USA). Filtering was carried out using PLINK (Software: https://www.cog-genomics.org/plink2). All individuals had missing call frequency < 0.1. SNPs with Hardy-Weinberg equilibrium exact test $p \geq 1 \times 10\text{-}6$, MAF $\geq$ 0.01 and genotyping rate > 0.99 were retained for analysis. After these filtering steps, 659 674 SNPs remained. Additional details of these analyses and the STREGA details are found in the original description of the cohort (Boardman *et al.*, 2014).

Preterm infant imaging genomics analysis of WNT pathway

A list of all genes in the *WNT* signalling pathway (entry hsa04310) in the Kyoto Encyclopaedia of Genes and Genomes (KEGG) was used as a gene-set-of-interest (n=141 genes). Gene-set analysis was carried out with the Joint Association of Genetic Variants (JAG) tool(Lips *et al.*, 2012; Lips *et al.*, 2015) to test the joint effect of all SNPs located in the WNT pathway. This procedure consists of three parts: 1) SNP to gene annotation; 2) self-contained testing (i.e. association) and 3) competitive testing (i.e. enrichment). An enriched pathway can be defined as one whose genes are more strongly associated with the phenotype than those genes outside the pathway. Phenotype permutation is used to evaluate gene-set significance, implicitly controlling for linkage disequilibrium, sample size, gene size, number of SNPs per gene, and

number of genes in a gene-set. This will result in a *p*-value (with a traditional significance threshold<0.05) if there is an enrichment for variants associated with the phenotype within the gene-set of interest compared to random matched gene-sets.

Following SNP-gene mapping, genes in the WNT-set were tested for association with the original phenotype (query data), and this was repeated with 1000 permutations of the phenotype (self-contained/association test). This association testing tests the null hypothesis that no pathway genes are associated with the phenotype and combines the individual gene association p-values into a single p-value for the entire pathway. The competitive/enrichment test was then done to test the null hypothesis that the pathway genes are no more associated with the phenotype than 300 randomly drawn non-pathway gene-sets, with 1000 phenotype permutations. The association analysis was repeated gene-by-gene within the *WNT* gene-set to investigate which members of the gene-set might be predominantly contributing to the collective signal.

Statistical analysis.

No statistical methods were used to predetermine sample sizes, but these were similar to those generally employed in the field. Data are expressed as the mean values +/- standard error of the mean (SEM). Data was first tested for normality using the Kolmogorov-Smirnov normality test for n=5-7 and D'Agostino & Pearson omnibus normality test for n>7. F-test (single comparisons) or Bartlett's test (multiple comparison) for analyse of variances was used. Multiple comparisons in the same data set were analysed by one-way ANOVA with Newman-Keuls *post hoc* test, Two-way ANOVA with Bonferroni *post hoc* or Kruskal-Wallis test with Dunns post hoc. Single comparisons to control were made using two-tailed Student's *t*-test or Mann-Whitney test. $P < 0.05$ was considered to be statistically significant. For the Barnes maze probe trial, univariate t test was performed to compare the % time spent in the target sextant to the theoretical value 16.67 % (i.e. when the mouse spent equal time within each sextant). Data handling and statistical processing was performed using Microsoft Excel and GraphPad Prism Software.

Results

MG activation drives hypomyelination in our model of encephalopathy of the premature infant

To understand the mechanisms underpinning encephalopathy of the premature infant in contemporaneous cohorts we previously set up a model mimicking its neuropathological, behavioural and imaging phenotypes(Favrais *et al.*, 2011; Krishnan *et al.*, 2017). Of note, the neuropathological similarities between our model and clinical studies includes MG/Mφ activation and hypomyelination due to the maturation blockade of oligodendrocytes but limited cell death(Billiards *et al.*, 2008; Verney *et al.*, 2010; Verney *et al.*, 2012). Specifically, intraperitoneal (i.p.) injections of interleukin (IL)-1β (10μg/kg) were administered to mouse pups twice daily on postnatal days (P) 1-4 and once at P5 (**Figure 1A**). P1-P5 in the mouse is a developmental period roughly corresponding to 22-32 weeks of human pregnancy(Marret *et al.*, 1995) and this is the greatest period of vulnerability for white matter damage in preterm born infants. Exposure to systemic IL-1β recapitulates the systemic inflammatory insult of maternal/fetal infections. Specifically, i.p. IL-1β injection causes a complex systemic response including increased blood levels of IL-6, TNFα and IL-1β(Favrais *et al.*, 2011) that lead to neuroinflammatory responses including microglial activation with increased cytokines and chemokines(Krishnan *et al.*, 2017; Shiow *et al.*, 2017). The eventual outcome being an oligodendrocyte maturation delay, that can be observed specifically as an increase in the numbers of NG2+ and PDGFRa+ OPC/pre-oligodendrocyte populations, decreased expression of MBP, MAG and MOG and altered axonal myelination into adulthood (Favrais *et al.*, 2011; Schang *et al.*, 2014; Shiow *et al.*, 2017) associated with cognitive dysfunction(Favrais *et al.*, 2011). In this study, we verified a direct causal link between MG/Mφ activation and neuropathology in our model by selectively killing pro-inflammatory MG/Mφ and observing a reduction in myelin injury. Specifically, we used an intracerebral injection of gadolinium chloride ($GdCl_3$), which kills pro-inflammatory MG/Mφ via competitive inhibition of calcium mobilization and damage to the plasma membrane. We validated *in vivo* that this approach is effective at reducing the numbers of pro-inflammatory microglia in the developing brain, and it has previously been validated *in vivo* in adult models of injury(Fulci *et al.*, 2007; Miron *et al.*, 2013; Du *et al.*, 2014). We chose this approach and not ablation of MG with a Tamoxifen driven transgenic or other pharmacologic approaches (i.e. PLX3397, ganciclovir) as our studies target maturing oligodendrocytes (as found in the preterm infant brain) that are present from P1. These conditional and pharmacologic depletion methods cannot practically be made effective at P1 and this window of development is key to this model. Also, embryonic depletion

of microglia itself alters brain development(Squarzoni *et al.*, 2014) in ways that would alter our experimental paradigm. $GdCl_3$ (200nmol) was injected into the corpus callosum of P1 mice prior to i.p injection of IL-1β or PBS. In the corpus callosum at P3, after 72 hours of exposure to systemic inflammation, immunohistological analysis revealed that the majority of MG/Mφ were IBA1+/COX2+ and the numbers of these cells was reduced by approximately 50% by $GdCl_3$ (**Figure 1B,C**). This $GdCl_3$-mediated reduction in MG/Mφ prevented the typical loss of myelin basic protein (MBP) in the corpus callosum at P30 (**Figure 1D,E**) but OLIG2 was not altered by exposure to systemic inflammation, as previously reported(Favrais *et al.*, 2011) or $GdCl_3$ (**Figure 1F,G)**. A link between microglial activation and hypomyelination can also be recapitulated with inflammatory activation of mixed glial cultures containing oligodendrocyte progenitor cells (OPCs), MG and astrocytes. In these *in vitro* conditions, there is reduced MBP+ cell density, without affecting the total number of oligodendrocytes (**Figure 1H)**. Exposure of pure OPC cultures (in the absence of microglia or astrocytes) to an inflammatory stimulant, IL-1β, did not cause hypomyelination (data not shown). Altogether, these results validate in our model a causal link between MG/Mφ activation and the hypomyelination that is a hallmark of encephalopathy of prematurity.

MG activation is persistent with specific temporal patterns in our model of encephalopathy of the preterm infant

We comprehensively characterized the morphology, gene and protein expression of MG/Mφ over time in our model to assess the relationship between activation states and injury. Our morphological analysis of GFP+ MG/Mφ from $CX3CR1^{GFP/+}$ mice revealed a moderate but significant reduction of complexity (arborisation) at P3 when comparing MG/Mφ from IL-1β versus PBS injected animals but no difference in process length or density, cell body area, numbers of primary, secondary and tertiary processes, or the area covered by the MG processes in 2D (**Figure 2A,B**). Cell morphology was measured at 3 hours after the first inflammatory challenge (at P1) and at P3 when animals had been exposed to >48 hours of systemic inflammation driven neuroinflammation in vibratome cut sections using a custom designed script developed with the Acapella™ image analysis(Verdonk *et al.*, 2016).

We further studied MG/Mφ activation using expression analysis of sixteen genes and six protein markers previously associated with polarized expression states(Chhor *et al.*, 2013; Miron *et al.*, 2013) at 5 time points. Gene expression analysis was performed in CD11B+ cells isolated by magnetically activated cell sorting (MACS, Miltenyi Biotec) from PBS- or IL-1β-exposed mice as per our previous studies(Chhor *et al.*, 2017; Krishnan *et al.*, 2017; Shiow *et*

al., 2017). Prior FACS analysis has demonstrated that the ratio of MG to other CD11B+ cells in this isolate is greater than 50 to 1(Krishnan *et al.*, 2017). Nevertheless, because we cannot exclude the presence of Mφ completely we use MG/Mφ as the descriptor for these cell isolates. Also, the purity of the MACS isolation was confirmed as >95% CD11B+ MG/Mφ by FACS and qRT-PCR, also as previously(Schang *et al.*, 2014; Krishnan *et al.*, 2017). qRT-PCR based gene expression analysis (**Figure 2C**) and immunofluorescence (**Supp Figure 1A-D**) showed that systemic exposure to IL-1β induced a robust pro-inflammatory MG/Mφ activation state at P1, only 3 hours following the first injection of IL-1β. Specifically, 5/6 markers of a pro-inflammatory state were significantly increased including *Il6* increased by 20-fold, and a 5-fold increases in *Ptgs2* and *Nos2*, all $p<0.001$. Of note, *Ptgs2* and *Nos2* remained elevated for 5 days, but *Il6* and *Tnfa* were returned to normal by P3. There was a similar robust increase in markers of immune-regulation at P1 as 4/4 markers were increased including an 8-fold increase in *Socs3* and >10-fold increase for *Sphk1* and *Il1rn*, all $p<0.001$. Expression of markers associated with an anti-inflammatory activation state were the most effected in animals exposed to systemic IL-1β exposure at P2 and P3, which is 48 or 72 hours after the start of IL-1β injections. These findings of a temporal change in MG/Mφ activation profiles were corroborated with immunohistological analysis of protein levels (**Supp Figure 1A-D**).

By combining our observations of morphology, gene and protein changes in MG/Mφ after systemic IL-1β exposure we have characterized a persistent state of activation responsible for injury to the developing white matter.

The Wnt pathway is comprehensively down-regulated in activated MG in vivo and in vitro

In mouse pups exposed to systemic IL-1β we have characterized a persistent activation of MG between P1 and until at least P5, which induces a partial blockade of OPC maturation and subsequently hypomyelination(Favrais *et al.*, 2011). Using gene and predicted protein network-based analysis, we sought to identify molecular pathways regulating this MG/Mφ activation driving OPC injury. We hypothesized that the best time to pick-up the potential disrupting regulator pathways specific to developing MG was P5 when MG are activated and when the first effects of OPCs have been observed and P10 when MG activation is apparently resolved but injury to OPCs is well established. As such, we undertook genome-wide transcriptomics analysis of MG/Mφ (CD11B+) and OPCs (O4+) MACSed at P5 and P10 from the brains of mice exposed to IL-1β or PBS. The purity of the O4+ MACS isolation was verified with qPCR(Schang *et al.*, 2014) as outlined for CD11B fractions above. Genes showing differential expression between time points, P5 and P10, were identified for each cell-type,

MG/Mφ (CD11B+) or OPCs (O4+), within each condition, IL-1β or PBS. Gene co-expression networks were inferred for each of the four sets of differentially expressed genes using Graphical Gaussian Models (GGMs)(Opgen-Rhein and Strimmer, 2007). GGMs use partial correlations to infer significant co-expression relationships. We applied a False Discovery Rate (FDR) of <1% between any microarray probe pair in each of the four sets of differentially expressed genes sets previously identified: PBS-OPC, IL-1β-OPC, PBS-MG/Mφ and IL-1β-MG/Mφ. These four co-expression networks were found to exhibit unique topologies and functional annotations (**Supp Figure 2A,B; Supp Tables 3 and 5**). Compared to the three other conditions networks, the IL-1β exposed MG/Mφ co-expression network was the most highly interconnected and the densest indicating a strong co-regulation of gene expression under this condition (**Supp Figure 2A,B)**. Biological pathway analysis using the Broad Institute MsigDB database(Subramanian *et al.*, 2005) indicated enrichment for Wnt signalling pathway genes within the IL-1β exposed MG/Mφ network (FDR=8.5 x 10^{-7}; **Figure 3A**; **Supp Table 3**). Due to the proposed importance of the Wnt pathway in OPC maturation(Fancy *et al.*, 2009) we undertook a specific analysis of data from the O4+ OPCs from mice subjected to systemic exposure to IL-1β. Analysis of microarray data from the O4+ OPCs did not show any significant enrichment for Wnt signalling genes in the gene co-expression response (**Supp Table 3**). This data highlight two important facts about Wnt dysregulation, firstly, that Wnt dysregulation is likely not a mechanism that directly effects oligodendrocytes in this model, and second, that changes in Wnt are not simply ubiquitous in the developing CNS in response to inflammation. Returning to the analysis of MG/Mφ, to highlight the directionality of the data, we looked for enrichments for Wnt signalling pathway sets among the genes significantly down-regulated by IL-1β exposure at P5 and P10 (**Supp Table 6**, see Methods). The known interactions among the Wnt pathway genes plus predicted interactors were then retrieved from an extensive set of functional association data by the GeneMania tool (Warde-Farley *et al.*, 2010) and we represented this sub-network (**Figure 3B**). We annotated this figure to highlight that the vast majority of targets predicted to interact in this model have down-regulated expression. Finally, qualitative gene profiling with qRT-PCR in CD11B+ MG/Mφ confirmed the down-regulation of mRNA expression for numerous Wnt pathway members including multiple Fzd receptors, *Lef1* and *Ctnnb1* in MG/Mφ from IL-1β-exposed mice (**Figure 3C).** The down-regulation of *Ctnnb1* mRNA was also accompanied by a significant decrease in the expression of β-catenin protein in CD11B+ MG/Mφ at P3 corresponding to the time point when the greatest morphological changes and pro-inflammatory gene activation is observed (**Figure 3D**).

To extend this *ex vivo* CD11B+ cell data and set up an *in vitro* model for further study, qRT-PCR and immunofluorescence analysis of mouse primary cultured MG was undertaken. The cultures are >97% pure for MG as validated with IHC and qRT-PCR, as previously reported(Chhor *et al.*, 2013). Exposure of MG to IL-1β *in vitro* induces a similar pro-inflammatory phenotype as is found in MG/Mφ from mice exposed to systemic IL-1β (**Supp Figure 3A,B** compared to data in **Figure 2C**). Furthermore, we observed a similar down-regulation of Wnt pathway members including mRNA encoding *Fzd* receptors, *Ctnnb1* and *Tcf1* (**Supp Figure 3C**). Inducing a pro-inflammatory activation in MG *in vitro* also induced an upregulation of mRNA encoding *Axin1* and *Axin2*, two specific inhibitors of β-catenin nuclear translocation (**Supp Figure 3C**) and reduced the protein levels for β-catenin as assessed with immunofluorescence (**Supp Figure 3D**), and ELISA (**Supp Figure 3E**). There was no significant change in the ratio of phosphorylated (Pser45) β-catenin to β-catenin also assessed with ELSIA (**Supp Figure 3E**). In contrast, IL-4, a classic anti-inflammatory stimulus, increased Wnt/β-catenin activation as indicated by strongly increased *Lef1* mRNA and decreased the Pser45 β-catenin/β-catenin ratio as measured via ELISA (**Supp Figure 3F,G**).

Altogether these data demonstrate that a pro-inflammatory MG/Mφ phenotype is associated with a robust and comprehensive down-regulation of the gene and protein expression of members of the Wnt/β-catenin signalling pathway *in vivo* and *in vitro*.

Wnt/β-catenin pathway activity negatively correlates with pro-inflammatory MG activation in vitro

We next sought to determine if Wnt/β-catenin pathway modulation alone is sufficient to drive phenotypic changes in MG *in vitro*. Pharmacological inhibition of the Wnt/β-catenin pathway *in vitro* with XAV939, a tankyrase inhibitor that stabilizes the Wnt/β-catenin pathway inhibitor Axin2(Fancy *et al.*, 2011), was sufficient to promote a pro-inflammatory phenotype, mimicking the effects of IL-1β (**Figure 3E**). Conversely, the IL-1β-induced pro-inflammatory MG phenotype was blocked by activating the Wnt pathway using siRNAs against Axin2 (**Figure 3F;** validation of siRNA efficacy **Supp Fig 3H**) or a pharmacological inhibitor of GSK3β that phosphorylates and inactivates β-catenin, CT99021(Ring *et al.*, 2003) (**Figure 3G**). As expected, we verified with ELISA that the Pser45 β-catenin/β-catenin ratio was increased with XAV939, and decreased with *Axin2* siRNA and CT99021 (**Figure 3H**). In contrast, we tested in PBS and IL-1β-exposed primary MG a non-isoform specific block of PKC signalling with Chelerythrine. Chelerythrine targets the non-canonical Wnt pathways and exposure of doses from 1-3μM had no effect on MG activation via qRT-PCR(**Supp Figure 4**). It is worth

noting that all pharmacologic approaches are liable to off target effects, but altogether the multiple compounds, and genetic targeting create a cohesive link to the Wnt canonical pathway as being key to MG activation.

Altogether, these data verify in pure cultures of primary MG that that modulating the Wnt/β-catenin pathway is sufficient and necessary to effect MG activation state.

*Wnt/*β-catenin *pathway activity negatively correlates with pro-inflammatory MG activation in vivo*

We further tested our working hypothesis that Wnt/β-catenin signalling drives a pro-inflammatory phenotype in MG/Mφ *in vivo* using non-cell specific approaches in zebrafish and mice and then transgenic mice with MG/Mφ specific β-catenin knock-down. In zebrafish larvae at 72 hours' post-fertilization (hpf) that express RFP in MG/Mφ (Tg[pU1::Gal4-UAS-TagRFP]) we injected into the hindbrain the prototypical pro-inflammatory agent lipopolysaccharide (LPS) (**Figure 4A**). LPS was used due to the unavailability of recombinant zebrafish IL-1β and prior work demonstrating the expression by zebrafish of receptors for LPS, the Toll-like 4 receptor (TLR4), and the requisite downstream signalling cascade(van der Sar *et al.*, 2006). Although LPS and IL-1β use differing signalling pathways, the end result of exposure to both is a complex neuroinflammatory milieu and it is this complex 'soup' (not the IL-1β alone. We compared the nature of the IL-1β and LPS responses in primary microglia using qRT-PCR for 12 genes to highlight the similarities in the overall inflammatory milieu induced by these inflammatory agents(see **Supp Figure 3A**), supporting our previous data comparing inflammatory protocols(Chhor *et al.*, 2013). LPS-induced neuroinflammation in the zebrafish was confirmed after 48 hours by a significant increase in fluorescent MG/Mφ in the optic tectum (**Figure 4B,C**). We observe a similar increase in MG/Mφ immunofluorescence in our mouse model with IBA1 and MAC1 immunofluorescence(Favrais *et al.*, 2011). As expected, exposure of zebrafish larvae to the Wnt/β-catenin antagonist XAV939 exacerbated the LPS-induced MG/Mφ activation, while conversely exposure to Wnt agonists acting via the canonical GSK3β dependent pathway with CT99021 or LiCl prevented the LPS induced MG/Mφ activation (**Figure 4B,C**).

Subsequently, we studied the specific relationship between Wnt/β-catenin pathway activity and MG/Mφ activation in mice using pharmacological and genetic approaches. Firstly, we inhibited the Wnt/β-catenin pathway by intracerebroventricular (i.c.v.) injection of XAV939 in P1 pups and isolated CD11B+ MG/Mφ 3 hours later. In agreement with our hypothesis, *in vivo* Wnt inhibition with XAV939 mimicked the effects of systemic IL-1β on gene expression

in MG/Mφ (**Figure 4D**). Furthermore, to specifically target the Wnt pathway in MG/Mφ, we bred LysM$^{Cre/Cre}$ with β-catenin$^{Flox/Flox}$ mice to generate β-Cat Δ /+ transgenic mice. Recombination, and as such KO, of β-catenin occurs in ≥20% of MG/Mφ in this Cre line(Cho *et al.*, 2008; Derecki *et al.*, 2012; Degos *et al.*, 2013) and we verified that there was 40% decrease in Ctnnb1mRNA encoding β-catenin ($P<0.001$, **Figure 4E**). In the absence of external inflammatory stimuli, β-Cat Δ /+ mice with MG expressing reduced levels of β-catenin developed a myelin deficiency that mimicked the damaging effects of systemic IL-1β exposure in our encephalopathy of prematurity model. Specifically, these mice had reduced *Mbp* mRNA in the anterior cortex at P10 (**Figure 4F**) and reduced MBP immunoreactivity in the corpus callosum and cingulum at P30 (**Figure 4G,H**).

Collectively, these data show that in fish and mice that down-regulation of the Wnt pathway is sufficient and necessary to drive a pro-inflammatory MG/Mφ activation state. Of note, even a partial MG/Mφ-specific β-catenin deletion *in vivo* in the absence of any external stimuli is sufficient to induce MG/Mφ activation leading to a myelination defect.

The Wnt pathway regulates activation state in primary human MG in vitro

We then verified a similar relationship between decreased Wnt and increased pro-inflammatory activation in primary human MACSed CD11B+ MG/Mφ isolated from cerebral tissues collected from scheduled terminations at 19- and 20-weeks' gestational age. Based on the low numbers of cells available we aimed to ensure we induced a robust response so we chose to use LPS to induce a pro-inflammatory MG response based on previous studies(Melief *et al.*, 2012). Human primary MG/Mφ were activated to a pro-inflammatory state as indicated by modified morphology (**Figure 5A**) and increased COX2 gene expression (*PTGS2* mRNA) (**Figure 5B**). In agreement with what we observed in our mouse and zebrafish experiments these pro-inflammatory activated human primary MG had a reduction in their expression of mRNA for the β-catenin gene, *CTNNB1* (**Figure 5C**).

Genomic variance in WNT pathway genes is relevant to human preterm infant white matter structure

Our experimental data show that genetic knockdown of Wnt/β-catenin signalling is sufficient itself to drive brain injury in transgenic mice. In a conceptually similar manner, but with an expected much smaller effect size, we reasoned that that genetic variation in *WNT* pathway genes would be associated with surrogates of white matter mediated connectivity in preterm born infants. We hypothesize that, at least in part, any link between WNT variation and

connectivity would be mediated by differences in the innate response to inflammatory challenge in these preterm infants. Although our genetic analysis is agnostic with respect to cellular mechanism or type, a link between WNT variations and brain structure would support further research into WNTs role in injury, and using WNT variants for preterm born infant injury/outcome stratification. To test our prediction of a link between WNT and preterm brain connectivity we performed an analysis where we jointly analysed connectivity data derived from MRI and genomics data from 290 preterm born infants. This approach has previously uncovered novel genetic variants associated with brain connectivity phenotype (Krishnan *et al.*, 2016; Krishnan *et al.*, 2017). The pre-term born infants included in this study are described in more detail in **Supp Table 4** and the inclusion/exclusion criteria are outlined in the materials and methods. Imaging of the white matter in preterm born infants associates with neurodevelopmental outcomes in preterm born infants (Woodward *et al.*, 2006; Spittle *et al.*, 2009; Pandit *et al.*, 2013), making an imaging-genomics approach relevant for generating hypotheses about the relevance of the WNT pathway to functional outcomes for preterm born infants.

In this paired imaging-genomics analysis, we assessed single nucleotide polymorphisms (SNPs) in our preterm cohort. SNPs are DNA sequence variations where a single nucleotide varies between individual members of a species that can help pinpoint contributions of specific genes to disease states. To define the intra-cerebral anatomical connectivity phenotype in our preterm cohort, we used 3-T dMRI and optimized probabilistic tractography as previously described(Robinson *et al.*, 2008; Shi *et al.*, 2011), adjusting the results for post-menstrual age at scan and at birth. Regions of interest for seeding tractography were obtained by segmentation of the brain based on a 90-node anatomical neonatal atlas(Shi *et al.*, 2011), focusing on cortico-cortical connections. DNA extracted from saliva was genotyped and a gene-set-of-interest defined using SNPs in the *WNT* signalling pathway (entry hsa04310) of the Kyoto Encyclopaedia of Genes and Genomes (KEGG) (n=141 genes).

SNPs were mapped to all of the genes in the KEGG WNT pathway using the JAG tool and Genome Reference Consortium Human Build 37 (GRCh37; hg19), using 2kb up/downstream, in line with NCBI practices (NCBI, 2005). Following SNP-gene mapping, we tested the null hypothesis that variation in WNT pathway genes is not associated with the preterm tractography phenotype using Joint Association of Genetic Variants (JAG)(Lips *et al.*, 2015). Specifically, genes in the WNT-set were tested in two ways (**Figure 5D**). Firstly, we performed a "competitive/enrichment test" to determine whether the *WNT* pathway genes were no more associated with the connectivity phenotype than 300 randomly drawn non-*WNT*-

pathway gene-sets. Secondly, we performed a "self-contained/association test" to determine whether there is a comparable association between the original connectivity phenotype and *WNT*, versus 1000 random permutations of the phenotype and *WNT*. The "competitive test", in which we compared to randomly generated sets of genes, showed a significant enrichment of genetic variants associated with the phenotype in the *WNT* gene-set compared to random gene sets (empirical p=0.037, **Figure 5E inset**). The conservative "self-contained" test in which we compared to 1,000 permutated phenotypes indicated that the WNT signalling gene-set was associated with our phenotype; i.e., white matter probabilistic tractography features (empirical p=0.064; **Figure 5E histogram & inset**). We performed a gene-by-gene analysis of SNPs within the *WNT* signalling gene-set to investigate which genes might be predominantly contributing to the collective pathway enrichment signal. This test highlighted a group of 10 genes with individual significant association with the tractography phenotype (empirical $p \leq 0.05$, 1,000 permutations). These ten genes included 8 associated with Wnt/β-catenin signalling *NFATC4*, *CSNK1A1*, *MAPK10*, *WNT2B*, *SMAD3*, *FBXW11*, *NLK*, *CSNK1A1L*, and 2 associated with the Wnt/Ca^{2+} or Wnt/PCP pathways, *PLCB2* and *WNT5A* (**Table 1; Supp Table 7**). Although, we cannot determine specifically how these SNP variants would alter the brain phenotype we found using the Genome-scale Integrated Analysis of gene Networks in Tissues ('GIANT') tool that these genes created a coherent interaction network within a human brain-specific gene interaction network (**Figure 5G; Supp Table 8**). GIANT hosts searchable genome-scale functional maps of human tissues, integrating an extensive collection of experimental data sets from publications including expression, regulatory and protein data(Greene *et al.*, 2015). We also performed an exploratory investigation of function for the 42 SNPs from the 10 genes predominantly contributing to the collective pathway enrichment signal to provide information related to function. We used the Gene Effect Predictor within the Consortium Human Build 37 (GRCh37; hg19) tool to study the 42 SNPs, whose full details are given in **Supp Table 9**. All 42 SNPs were existing in the database and they were predicted to have 463 consequences on the genome (**Supp Table 10**). Specifically, these SNPs overlapped with 103 separate gene transcripts, 7 of them overlapped regulatory sequences and overall 95% were synonymous variants and 5% were missense variants (**Figure 5F).**

These linked imaging-genomic analyses demonstrate a relationship between genetic variation in the WNT pathway with an important clinical phenotype. They provide adjunct support for a causal relationship between the Wnt pathway and the brain phenotype that has been established with our experimental data.

A Wnt pathway agonist delivered specifically to MG by a nanocarrier in vivo prevents neuroinflammation-mediated hypomyelination and the associated cognitive impairment

There is a paucity of neurotherapeutic options for damage to the preterm born infant brain and many other neuroinflammatory-mediated neurological disorders. We have clearly demonstrated a link between decreased Wnt/β-catenin pathway activation and a pro-inflammatory MG activation state. In addition, we have shown the relevance of this pathway in human MG and preterm infant brain structure. As such, we complete this study by demonstrating that the Wnt pathway is a viable therapeutic target. To achieve this, we specifically increased Wnt pathway activity in MG/Mφ using a peptide inhibitor of GSK3β, which has the effect of preventing the formation of the β-catenin degradation complex. We delivered this peptide to MG/Mφ *in vitro* and *in vivo* by conjugating it to a 3DNA nanocarrier together with a fluorescent tag (Cy3)(Genisphere, PA, USA). 3DNA nanocarriers are interconnected monomeric subunits of DNA of approximately 200nM in diameter that are intrinsically capable of endosomal escape(Muro, 2014). In brief, we validated that our 3DNA-peptide conjugate had MG specificity and immunomodulatory efficacy *in vitro*, that is crosses the BBB, that it has cell specificity *in vivo,* and finally that it is neurotherapeutic *in vivo* in our systemic-inflammation (IL-1β) driven model of encephalopathy of the preterm born infant.

First, we demonstrated *in vitro* that 3DNA nanocarrier Cy3 tagged conjugates are specifically internalized by MG in mixed glial cultures (**Supp Figure 5A)** and by MG in primary cultures after 4 hours of incubation (**Supp Figure 5B**). When 3DNA was conjugated to both Cy3 and the peptide L803mts, an agonist of canonical Wnt signalling via inhibition of GSK3β, it was also specifically internalized by MG in primary culture (**Supp Figure 6A**). We also used the 3DNA nanocarrier tagged with Cy3 to deliver a cargo of L803mts to MG/Mφ that had been activated with IL-1β *in vitro*. Treatment of primary MG with L803mts delivered with 3DNA reversed the IL-1β-induced activation of the MG but had no effect on PBS-treated MG as assessed with gene expression analysis (**Supp Figure 6B**).

Moving *in vivo*, we aimed to generate the proof-of-concept that the 3DNA nanocarrier delivering L803mts and tagged with Cy3 can be taken up by MG/Mφ and influence MG/Mφ phenotype. Specifically, the L803mts and Cy3 conjugated 3DNA nanocarrier or the scrambled (SCR) peptide control and Cy3 conjugated 3DNA nanocarrier was injected i.c.v. into P1 mice, 1 hour prior to our standard i.p. IL-1β injection. Four hours after i.c.v. injection, we observed Cy3 fluorescence exclusively co-localized with IBA-1+ staining in the periventricular white matter (**Figure 6A, Supp video 1**). In the same paradigm, using qRT-PCR analysis of isolated CD11B+ MG/Mφ we demonstrated that i.c.v. delivered 3DNA loaded with L803mts and tagged

with Cy3 reversed the effect of IL-1β on the MG/Mφ phenotype but that the 3DNA-L803mts-Cy3 had no significant effect on MG/Mφ from PBS-treated mice (**Figure 6B**). As i.c.v. injections cause aggravated tissue injury we subsequently undertook a translationally orientated trial using i.p. delivery of Cy3-tagged 3DNA conjugated to L803mts. The 3DNA L803mts Cy3 or 3DNA SCR Cy3 control was injected i.p. daily between P1 and P5, in parallel with PBS or IL-1β. At P5, immunofluorescence in the anterior periventricular white matter confirmed that 3DNA L803 mts Cy3 was specifically taken up by IBA1+ MG/Mφ (**Figure 7A**). We also assessed uptake of our 3DNA conjugate by populations of macrophage in the body after i.p. delivery at P5. Using the same IHC techniques that clearly shows uptake in MG/Mφ we did not find Cy3 positive staining in the spleen or liver (**Supp Figure 5C,D**).

To validate the *in vivo* neurotherapeutic efficacy of our novel nanocarrier-mediated WNT agonist therapy, we assessed the IL-1β-induced myelination deficit by measuring *Mbp* mRNA at P10, MBP protein via western blotting at P15 and axonal myelination via electron microscopy at P30. We have previously shown in this model that there is an accumulation of immature oligodendrocytes (NG2+ and PDGFRa+), reduced small calibre axonal myelination and reduced expression of myelin proteins(Favrais *et al.*, 2011; Schang *et al.*, 2014; Rangon *et al.*, 2018).Treatment with i.p. 3DNA L803mts Cy3 significantly prevented the IL-1β-induced reduction in *Mbp* mRNA (**Figure 7B**) and alleviated the IL-1β-induced reduction in MBP proteins **(Figure 7C,D, Supp Figure 7A)**. Finally, we observed that these effects of 3DNA L803mt Cy3 to improve MBP mRNA and MBP protein levels correlated with improvements in axonal myelination, as indicated by the decrease of G-ratio of fibres of 0.2 to 0.8μm diameter in the corpus collosum (**Figure 7E,F**).

In order to evaluate whether this improvement in neuropathology with nanocarrier mediated treatment also reverses the behavioural deficits observed in adults in this paradigm, spatial learning and memory were assessed starting at P90. Basic behavioural parameters we first tested via spontaneous locomotion and rearing using actimetry and exploratory behaviour with an open field test. This injury model is designed to induce subtle neurobehavioral deficits to mimic the learning problems that become apparent in school age children born preterm(Lindstrom *et al.*, 2011; Spittle *et al.*, 2017). As expected, no changes in these basic parameters was observed between groups of mice., i.e. controls (PBS+3DNA SCR Cy3), injured (IL-1β+SRC Cy3) or the treatment group (IL-1β+3DNA L803mts Cy3) (**Supp Figure 7B,C**). Spatial learning and memory were tested via the Barnes maze test, which assesses spatial learning over 5 days of probe trials plus short term memory retention at the end of the learning trials and long term memory retention 10 days later. Spatial learning (i.e., distance travelled

and number of errors) itself was not modified by IL-1β exposure (**Figure 7G**). However, mice exposed to IL-1β had a short-term memory deficit based on a decreased distance travelled in the target sextant during the first 30 seconds of the probe trial on the final day of testing (**Figure 7H**). In addition, IL-1β exposure caused deficits in long term memory recall, as assessed as the increased distance travelled in a single probe trial at 10 days post-learning (**Figure 7I**). These short term and long term neuroinflammatory induced memory deficits were both reversed by i.p. treatment by delivery to MG/Mφ of the Wnt antagonist, L803 mts (3DNA L803 mts Cy3) by the 3DNA nanocarrier (**Figure 6H,I**).

Altogether these data clearly demonstrate that a Wnt agonist therapy can reduce pro-inflammatory MG/Mφ activation and improve neuropathological and functional outcomes in a model of neuroinflammation mediated white matter injury. These data also highlight a novel 3DNA nanocarrier that has the ability to deliver therapies like this *in vivo* specifically to MG.

Discussion

Recent research has highlighted that microglia of the developing brain have a unique phenotype. The aims of this study were, the identification in MG of the developing brain of the molecular regulators of injury-related phenotype, and validation of these as therapeutic targets for preventing microglia-mediated injury in the 15 million infants born preterm every year. We undertook a comprehensive set of studies involving pharmacologic and genetic manipulations in mouse and zebrafish models, human tissue and patient data. We also introduced an innovative 3DNA nanocarrier that can deliver drugs specifically to microglia *in vivo*. Initially, we characterised the complex MG/Mφ phenotype in our mouse model of encephalopathy of prematurity(Favrais *et al.*, 2011; Schang *et al.*, 2014; Krishnan *et al.*, 2017) and demonstrated that MG/Mφ activation is directly responsible in this model for the clinically relevant myelination defect. Next, using a genome-wide transcriptomic analysis of these activated MG/Mφ we associated the Wnt pathway with MG/Mφ activation. We specifically determined that the expression of Wnt/β-catenin pathway receptors, ligands and intracellular signalling components were robustly down-regulated in MG/Mφ isolated from our animal model. A combination of approaches in zebrafish and mouse models *in vitro* and *in vivo* allowed us to determine that Wnt/β-catenin pathway inhibition specific to MG/Mφ is sufficient and necessary to induce in these cells a pro-inflammatory activation, and subsequent hypomyelination *in vivo*. We highlighted the relevance of the *WNT* pathway to the activation state of human primary MG, and preterm born infant brain development. Of note, we verified our prediction that genetic variation in the *WNT* pathway in preterm infants is related to indices of their cerebral structural connectivity. Although, it is a limitation of these types of human studies that the data is not cell specific and the effects of the WNT SNPs may be on earlier stages of development in other cell types. Finally, we selectively delivered to MG/Mφ *in vivo* a Wnt pathway activator using a 3DNA nanocarrier, which we administered via non-invasive i.p. injection. This specific and non-invasive delivery of a Wnt agonist therapeutic prevented a pro-inflammatory MG/Mφ activation state and the associated white matter damage and cognitive deficit in our mouse model. Together, these data demonstrate that down-regulation of the canonical Wnt/β-catenin pathway triggers a hypomyelination-inducing MG phenotype and validate this pathway as a novel and clinically viable neurotherapeutic target thanks to the MG/Mφ-specificity of 3DNA nanocarriers.

Our evidence supports that the Wnt pathway controlling MG/Mφ phenotype is the canonical Wnt/β-catenin pathway. Our supporting data include that genetic and

pharmacological manipulation of the β-catenin degradation complex via Axin2 robustly effected MG/Mφ phenotype *in vitro* and *in vivo*. In contrast, blockade of non-canonical Wnt signalling with a PKC inhibitor had no effect on MG activation. Although, we acknowledge that there may still be a role for other facets of non-canonical signalling in the complexity of MG/Mφ functions. However, MG/Mφ-specific β-catenin ablation *in vivo* in-of-itself was sufficient to recapitulate the systemic-inflammation-driven hypomyelination that we see in our animal model of encephalopathy of prematurity. We also found that the WNT genes with variance associated with preterm infant connectivity were predominantly (8/10) from the Wnt/β-catenin pathway. A key role for β-catenin would also begin to explain our observations of Wnt-mediated pro-inflammatory activation via TLR-4 and IL-1 receptor agonists and also conversely Wnt-mediated anti-inflammatory activation via a IL-4 receptor agonist. Down-stream signalling of both the TLR/IL-1 and IL-4 receptor families includes activation of the transcription factor NF- κB (nuclear factor kappa-light-chain-enhancer of activated B cells)(Caamano and Hunter, 2002). The ability of NF-κB to mediate the opposing effects of these receptors on MG phenotype is conferred by interactions with other regulatory factors, including at multiple levels indirectly and directly by β-catenin(Ma and Hottiger, 2016).

Ours is the first study to demonstrate a robust cell-intrinsic role of the Wnt/β-catenin pathway in MG activation *in vitro* and *in vivo* and validate that this pathway is a viable immunomodulatory neurotherapeutic. Previous work on Wnt and MG has been limited to *in vitro* ligand-receptor interactions, specifically WNT3a or WNT5a. However, the specific Wnt pathway activated by a Wnt ligand is dependent on the context of ligand-receptor interaction not only cell-intrinsic properties(van Amerongen *et al.*, 2008). This fact likely explains the discordance between the data from the previous studies, where in some paradigms Wnt exposure is anti-inflammatory(Halleskog *et al.*, 2012; Yu *et al.*, 2014) or in others the exposure was pro-inflammatory(Halleskog *et al.*, 2011; Hooper *et al.*, 2012; Halleskog and Schulte, 2013) with no relation to the predicted canonical or non-canonical pathway being activated. Altogether these data highlight the difficulty that would be faced in using ligand-receptor interactions to target the Wnt pathway to modulate MG activity, in contrast with our success of targeting the intracellular cascade of Wnt/β-catenin pathway specifically using our 3DNA-mediated delivery system. We also wish to note that the Wnt pathway has well characterised roles in oligodendrocyte maturation(Fancy *et al.*, 2011; Feigenson *et al.*, 2011; Guo *et al.*, 2015; Zhao *et al.*, 2016), astrocyte activation(Cao *et al.*, 2012) and endothelial cell function(Lengfeld *et al.*, 2017). Our study builds on this understanding of the role of Wnt as a complex cell specific temporally and spatially regulated controller of brain development and response to injury.

The 3DNA nanocarrier is a powerful translational tool as is it can take agents across the BBB following i.p. injection, is specifically internalized by MG/Mφ in the brain and it has no toxicity *in vitro* or *in vivo* in our study, or in human retinal tissue *in vitro*(Gerhart *et al.*, 2017) and in pre-clinical *in vivo* targeted delivery of a ovarian cancer therapy(Huang *et al.*, 2016). Wnt activation in OPCs has previously been suggested to block their maturation by a member of our current research team(Fancy *et al.*, 2011). As such it was important that 3DNA-nanocarriers allowed us to target this pathway exclusively in MG/Mφ. 3DNA has a non-injury dependent mechanism of traversing the BBB, as it crossed in naïve and inflammation-exposed mice, although the specific mechanism is unknown. We have previously reported that the BBB in our mouse model of encephalopathy of prematurity is primarily intact(Krishnan *et al.*, 2017). The chemical and physical attributes of 3DNA likely precludes it from entering the brain via paracellular aqueous routes or transcellular lipophilic pathways. However, investigations of receptor mediated transcytosis are underway, as similar aptamer-based DNA duplexes can interact with receptors such as nucleolin or transferrin(Reyes-Reyes *et al.*, 2010).

In preterm infants, it is exposure to inflammatory events that are both difficult to identify or prevent, such as chorioamnionitis and sepsis, that is the leading risk factor for white matter damage. This damage is caused by microglia-mediated neuroinflammatory processes a link that is supported by post-mortem human studies showing microgliosis in the developing white matter of preterm born infants (Verney *et al.*, 2010; Verney *et al.*, 2012; Supramaniam *et al.*, 2013) and verified by numerous experimental paradigms(see references in, Hagberg *et al.*, 2015). White matter damage in these infants is observed as diffuse white matter signal changes and reduced structural connectivity using MRI analyses(Shah *et al.*, 2008; Spittle *et al.*, 2009). In a large animal model of preterm born infant brain injury a direct link between diffuse white matter injury and white matter gliosis has been made(Riddle *et al.*, 2011). This reduced structural connectivity in preterm born infants is in turn strongly associated with poor neurodevelopmental outcomes(Woodward *et al.*, 2006; Ball *et al.*, 2015). As such, the purpose of our imaging-genomics analysis was to link the pre-clinical observations of microglial mediated compromise of structural connectivity due to white matter injury to genetic variance that could alter the microglial inflammatory response in our preterm cohort and would affect changes in structural connectivity. Our integrated analysis of imaging and genomics demonstrated that common genetic variation in *WNT* pathway genes does indeed influence brain structural connectivity features within our preterm born infants. We fully acknowledge that the data we derived is not cell specific and could be due to effects on the white and grey matter. However, it supports in contemporaneous infants the relevance of the *WNT* pathway

using an imaging modality that is currently used to assess injury and predict outcome. Also, we wish to highlight that changes to the grey matter are also evident in preterm born infants, including changes in cortical microstructure(Ball *et al.*, 2013), interneuron distribution(Stolp *et al.*, 2019) and degeneration of axons(Back and Miller, 2014). However, the contribution of axonal injury to diffuse white matter is controversial, although it is evident in necrotic foci that are approximated to occur in only 5% of white matter injury cases(Riddle *et al.*, 2011; Buser *et al.*, 2012). Preterm born infants with apparent focal necrosis were excluded from our imaging-genomics analysis removing a significant contribution of a frank axonopathy from effecting the connectivity phenotype in this cohort. We cannot exclude however that effects on the grey matter in these infants are not important determiners of outcome and effected by changes in SNPs in genes of the WNT pathway. In addition, we found that the *WNT* pathway genes containing SNPs associated with white matter tractography phenotype belonged to a human brain-specific gene interaction network. This network further builds a case for a functional effect of *WNT* SNPs in human preterm infants, with consequences for the development of white matter structure(Greene *et al.*, 2015). Specific prediction of the consequences of our identified SNPs found the majority were intron variants. Previous studies in experimental animals has shown that immune cell intron variants often effect cell function by altering enhancer binding(Farh *et al.*, 2015). Altogether our clinical data build a case that these *WNT* pathway SNPs may be a useful way to stratify infants who are at highest risk for white matter damage, and to improve on our currently limited prognostic abilities related to long term outcome.

In conclusion, the activity of the Wnt/β-catenin pathway regulates MG/Mφ activation, the Wnt pathway is relevant in human brain development, and specific agonism of the Wnt/β-catenin pathway in MG/Mφ *in vivo* using 3DNA nanocarrier-mediated drug-delivery has a beneficial effect on MG/Mφ phenotype, myelination and cognitive deficits. This is strong evidence that Wnt signalling modulation may be a promising therapeutic approach in encephalopathy of prematurity and, potentially, in other disorders involving MG/Mφ-mediated neuroinflammation.

Declaration of authorship

J.V.S., A.L.S., M.K., F.V., V.D., O.H., S.L., L.S., T.L.C., G.B., P.A., A.S., C.A., V.M.; D.R., F.C., C.L., V.B., E.G.P., A.D.E., H.H., N.S.Y., B.F., P.G. designed the research; J.V.S., A.L.S., M.L. K., Z.C., S.S., A.M., F.V., O.H., C.B., A.D., S.L., L.S., T.L.C., R.H.A., G.B., P.A., A.S., R.K.H., C.A., V.M., C.L., V.B., N.S.Y., B.F., P.G. performed the research; W.B. provided the β-catenin floxed mice; J.V.S., A.L.S., M.L.K., Z.C., S.S., A.M., F.V., V.D., O.H., S.L., L.S., T.L.C., R.H.A., G.B., O.B., P.A., A.S., C.A., V.M., C.B., A.D., D.R., F.C., C.L., V.B., E.G.P., A.D.E., H.H.H, N.S.Y., B.F., P.G. analysed the data; J.V.S., M.L.K., O.B., D.R., FC., C.B., A.D., C.L., V.B., E.G.P., A.D.E., H.H, N.S.Y., B.F., P.G. wrote the manuscript.

Data availability. All new data are available from the authors on request, subject to ethical restrictions related to the human studies.

Acknowledgments

Our thanks to the children and families who participated in the study, and the nurses, doctors and scientists who supported the project. This study was supported by grants from Inserm, Université Paris Diderot, Université Sorbonne-Paris-Cité, Investissement d'Avenir (ANR-11-INBS-0011, NeurATRIS), ERA-NET Neuron (Micromet), DHU PROTECT, Association Robert Debré, PremUP, Fondation de France, Fondation pour la Recherche sur le Cerveau, Fondation des Gueules Cassées, Roger de Spoelberch Foundation, Grace de Monaco Foundation, Leducq Foundation, Action Medical Research, Cerebral Palsy Alliance Research Foundation Australia, Wellcome Trust (WSCR P32674) and The Swedish Research Council (2015-02493). We wish to acknowledge the support of the Department of Perinatal Imaging and Health, King's College London. In addition, the authors acknowledge financial support from the National Institute for Health Research (NIHR) Biomedical Research Centre based at Guy's and St Thomas' NHS Foundation Trust and King's College London. The views expressed are those of the author(s) and not necessarily those of the NHS, the NIHR or the Department of Health. We also wish to thank Dr Dominique Langui (Institut du Cerveau et de la Moelle épinière, Hôpital Pitié-Salpêtrière, Paris, France) for providing us with access to electron microscopy facilities and Dr Manuela ZinniI INSERM U1141 NeuroDiderot for access to additional molecular biology facilities.

References

Back SA, Luo NL, Mallinson RA, O'Malley JP, Wallen LD, Frei B*, et al.* Selective vulnerability of preterm white matter to oxidative damage defined by F2-isoprostanes. Ann Neurol 2005; 58(1): 108-20.

Back SA, Miller SP. Brain injury in premature neonates: A primary cerebral dysmaturation disorder? Ann Neurol 2014; 75(4): 469-86.

Ball G, Counsell SJ, Anjari M, Merchant N, Arichi T, Doria V*, et al.* An optimised tract-based spatial statistics protocol for neonates: applications to prematurity and chronic lung disease. Neuroimage 2010; 53(1): 94-102.

Ball G, Pazderova L, Chew A, Tusor N, Merchant N, Arichi T*, et al.* Thalamocortical Connectivity Predicts Cognition in Children Born Preterm. Cereb Cortex 2015; 25(11): 4310-8.

Ball G, Srinivasan L, Aljabar P, Counsell SJ, Durighel G, Hajnal JV*, et al.* Development of cortical microstructure in the preterm human brain. Proc Natl Acad Sci U S A 2013; 110(23): 9541-6.

Bennett ML, Bennett FC, Liddelow SA, Ajami B, Zamanian JL, Fernhoff NB*, et al.* New tools for studying microglia in the mouse and human CNS. Proc Natl Acad Sci U S A 2016; 113(12): E1738-46.

Billiards SS, Haynes RL, Folkerth RD, Borenstein NS, Trachtenberg FL, Rowitch DH*, et al.* Myelin abnormalities without oligodendrocyte loss in periventricular leukomalacia. Brain Pathol 2008; 18(2): 153-63.

Boardman JP, Walley A, Ball G, Takousis P, Krishnan ML, Hughes-Carre L*, et al.* Common genetic variants and risk of brain injury after preterm birth. Pediatrics 2014; 133(6): e1655-63.

Buchanan FG, DuBois RN. Connecting COX-2 and Wnt in cancer. Cancer Cell 2006; 9(1): 6-8.

Buser JR, Maire J, Riddle A, Gong X, Nguyen T, Nelson K*, et al.* Arrested preoligodendrocyte maturation contributes to myelination failure in premature infants. Ann Neurol 2012; 71(1): 93-109.

Butovsky O, Jedrychowski MP, Moore CS, Cialic R, Lanser AJ, Gabriely G*, et al.* Identification of a unique TGF-beta-dependent molecular and functional signature in microglia. Nat Neurosci 2014; 17(1): 131-43.

Caamano J, Hunter CA. NF-kappaB family of transcription factors: central regulators of innate and adaptive immune functions. Clin Microbiol Rev 2002; 15(3): 414-29.

Cao F, Yin A, Wen G, Sheikh AM, Tauqeer Z, Malik M*, et al.* Alteration of astrocytes and Wnt/beta-catenin signaling in the frontal cortex of autistic subjects. J Neuroinflammation 2012; 9: 223.

Chhor V, Le Charpentier T, Lebon S, Ore MV, Celador IL, Josserand J*, et al.* Characterization of phenotype markers and neuronotoxic potential of polarised primary microglia in vitro. Brain Behav Immun 2013; 32: 70-85.

Chhor V, Moretti R, Le Charpentier T, Sigaut S, Lebon S, Schwendimann L*, et al.* Role of microglia in a mouse model of paediatric traumatic brain injury. Brain Behav Immun 2017; 63: 197-209.

Cho IH, Hong J, Suh EC, Kim JH, Lee H, Lee JE*, et al.* Role of microglial IKKbeta in kainic acid-induced hippocampal neuronal cell death. Brain 2008; 131(Pt 11): 3019-33.

Dammann O, Leviton A. Inflammatory brain damage in preterm newborns--dry numbers, wet lab, and causal inferences. Early Hum Dev 2004; 79(1): 1-15.

Degos V, Peineau S, Nijboer C, Kaindl AM, Sigaut S, Favrais G, *et al.* G protein-coupled receptor kinase 2 and group I metabotropic glutamate receptors mediate inflammation-induced sensitization to excitotoxic neurodegeneration. Ann Neurol 2013; 73(5): 667-78.

Delobel-Ayoub M, Arnaud C, White-Koning M, Casper C, Pierrat V, Garel M, *et al.* Behavioral problems and cognitive performance at 5 years of age after very preterm birth: the EPIPAGE Study. Pediatrics 2009; 123(6): 1485-92.

Derecki NC, Cronk JC, Lu Z, Xu E, Abbott SB, Guyenet PG, *et al.* Wild-type microglia arrest pathology in a mouse model of Rett syndrome. Nature 2012; 484(7392): 105-9.

Du C, Wang P, Yu Y, Chen F, Liu J, Li Y. Gadolinium chloride improves the course of TNBS and DSS-induced colitis through protecting against colonic mucosal inflammation. Sci Rep 2014; 4: 6096.

Durinck S, Spellman PT, Birney E, Huber W. Mapping identifiers for the integration of genomic datasets with the R/Bioconductor package biomaRt. Nature protocols 2009; 4(8): 1184-91.

Fancy SP, Baranzini SE, Zhao C, Yuk DI, Irvine KA, Kaing S, *et al.* Dysregulation of the Wnt pathway inhibits timely myelination and remyelination in the mammalian CNS. Genes Dev 2009; 23(13): 1571-85.

Fancy SP, Harrington EP, Baranzini SE, Silbereis JC, Shiow LR, Yuen TJ, *et al.* Parallel states of pathological Wnt signaling in neonatal brain injury and colon cancer. Nat Neurosci 2014; 17(4): 506-12.

Fancy SP, Harrington EP, Yuen TJ, Silbereis JC, Zhao C, Baranzini SE, *et al.* Axin2 as regulatory and therapeutic target in newborn brain injury and remyelination. Nat Neurosci 2011; 14(8): 1009-16.

Farh KK, Marson A, Zhu J, Kleinewietfeld M, Housley WJ, Beik S, *et al.* Genetic and epigenetic fine mapping of causal autoimmune disease variants. Nature 2015; 518(7539): 337-43.

Favrais G, van de Looij Y, Fleiss B, Ramanantsoa N, Bonnin P, Stoltenburg-Didinger G, *et al.* Systemic inflammation disrupts the developmental program of white matter. Ann Neurol 2011; 70(4): 550-65.

Feigenson K, Reid M, See J, Crenshaw EB, 3rd, Grinspan JB. Wnt signaling is sufficient to perturb oligodendrocyte maturation. Mol Cell Neurosci 2009; 42(3): 255-65.

Feigenson K, Reid M, See J, Crenshaw IE, Grinspan JB. Canonical Wnt signalling requires the BMP pathway to inhibit oligodendrocyte maturation. ASN Neuro 2011; 3(3): e00061.

Fulci G, Dmitrieva N, Gianni D, Fontana EJ, Pan X, Lu Y, *et al.* Depletion of peripheral macrophages and brain microglia increases brain tumor titers of oncolytic viruses. Cancer Res 2007; 67(19): 9398-406.

Gentleman RC, Carey VJ, Bates DM, Bolstad B, Dettling M, Dudoit S, *et al.* Bioconductor: open software development for computational biology and bioinformatics. Genome Biol 2004; 5(10): R80.

Gerhart J, Greenbaum M, Casta L, Clemente A, Mathers K, Getts R, *et al.* Antibody-Conjugated, DNA-Based Nanocarriers Intercalated with Doxorubicin Eliminate Myofibroblasts in Explants of Human Lens Tissue. J Pharmacol Exp Ther 2017; 361(1): 60-7.

Greene CS, Krishnan A, Wong AK, Ricciotti E, Zelaya RA, Himmelstein DS, *et al.* Understanding multicellular function and disease with human tissue-specific networks. Nat Genet 2015; 47(6): 569-76.

Guo F, Lang J, Sohn J, Hammond E, Chang M, Pleasure D. Canonical Wnt signaling in the oligodendroglial lineage--puzzles remain. Glia 2015; 63(10): 1671-93.

Hagberg H, Gressens P, Mallard C. Inflammation during fetal and neonatal life: implications for neurologic and neuropsychiatric disease in children and adults. Ann Neurol 2012; 71(4): 444-57.

Hagberg H, Mallard C. Effect of inflammation on central nervous system development and vulnerability. Curr Opin Neurol 2005; 18(2): 117-23.

Hagberg H, Mallard C, Ferriero DM, Vannucci SJ, Levison SW, Vexler ZS*, et al.* The role of inflammation in perinatal brain injury. Nat Rev Neurol 2015; 11(4): 192-208.

Halleskog C, Dijksterhuis JP, Kilander MB, Becerril-Ortega J, Villaescusa JC, Lindgren E*, et al.* Heterotrimeric G protein-dependent WNT-5A signaling to ERK1/2 mediates distinct aspects of microglia proinflammatory transformation. J Neuroinflammation 2012; 9: 111.

Halleskog C, Mulder J, Dahlstrom J, Mackie K, Hortobagyi T, Tanila H*, et al.* WNT signaling in activated microglia is proinflammatory. Glia 2011; 59(1): 119-31.

Halleskog C, Schulte G. WNT-3A and WNT-5A counteract lipopolysaccharide-induced pro-inflammatory changes in mouse primary microglia. J Neurochem 2013; 125(6): 803-8.

Hamrick SE, Miller SP, Leonard C, Glidden DV, Goldstein R, Ramaswamy V*, et al.* Trends in severe brain injury and neurodevelopmental outcome in premature newborn infants: the role of cystic periventricular leukomalacia. J Pediatr 2004; 145(5): 593-9.

Haynes RL, Billiards SS, Borenstein NS, Volpe JJ, Kinney HC. Diffuse axonal injury in Periventricular Leukomalacia as determined by apoptotic marker fractin. Pediatr Res 2008; 63(6): 656-61.

Hickman S, Izzy S, Sen P, Morsett L, El Khoury J. Microglia in neurodegeneration. Nat Neurosci 2018; 21(10): 1359-69.

Hillier SL, Witkin SS, Krohn MA, Watts DH, Kiviat NB, Eschenbach DA. The relationship of amniotic fluid cytokines and preterm delivery, amniotic fluid infection, histologic chorioamnionitis, and chorioamnion infection. Obstet Gynecol 1993; 81(6): 941-8.

Hooper C, Sainz-Fuertes R, Lynham S, Hye A, Killick R, Warley A*, et al.* Wnt3a induces exosome secretion from primary cultured rat microglia. BMC neuroscience 2012; 13: 144.

Huang YH, Peng W, Furuuchi N, Gerhart J, Rhodes K, Mukherjee N*, et al.* Delivery of Therapeutics Targeting the mRNA-Binding Protein HuR Using 3DNA Nanocarriers Suppresses Ovarian Tumor Growth. Cancer Res 2016; 76(6): 1549-59.

Johnston MV, Hagberg H. Sex and the pathogenesis of cerebral palsy. Dev Med Child Neurol 2007; 49(1): 74-8.

Kaidanovich-Beilin O, Eldar-Finkelman H. Long-term treatment with novel glycogen synthase kinase-3 inhibitor improves glucose homeostasis in ob/ob mice: molecular characterization in liver and muscle. J Pharmacol Exp Ther 2006; 316(1): 17-24.

Keats EC, Dominguez JM, 2nd, Grant MB, Khan ZA. Switch from canonical to noncanonical Wnt signaling mediates high glucose-induced adipogenesis. Stem cells (Dayton, Ohio) 2014; 32(6): 1649-60.

Krasemann S, Madore C, Cialic R, Baufeld C, Calcagno N, El Fatimy R*, et al.* The TREM2-APOE Pathway Drives the Transcriptional Phenotype of Dysfunctional Microglia in Neurodegenerative Diseases. Immunity 2017; 47(3): 566-81 e9.

Krishnan ML, Van Steenwinckel J, Schang AL, Yan J, Arnadottir J, Le Charpentier T*, et al.* Integrative genomics of microglia implicates DLG4 (PSD95) in the white matter development of preterm infants. Nat Commun 2017; 8(1): 428.

Krishnan ML, Wang Z, Silver M, Boardman JP, Ball G, Counsell SJ*, et al.* Possible relationship between common genetic variation and white matter development in a pilot study of preterm infants. Brain Behav 2016; 6(7): e00434.

Lengfeld JE, Lutz SE, Smith JR, Diaconu C, Scott C, Kofman SB*, et al.* Endothelial Wnt/beta-catenin signaling reduces immune cell infiltration in multiple sclerosis. Proc Natl Acad Sci U S A 2017; 114(7): E1168-E77.

Lim SS, Vos T, Flaxman AD, Danaei G, Shibuya K, Adair-Rohani H*, et al.* A comparative risk assessment of burden of disease and injury attributable to 67 risk factors and risk factor clusters in 21 regions, 1990-2010: a systematic analysis for the Global Burden of Disease Study 2010. Lancet 2012; 380(9859): 2224-60.

Lindstrom K, Lindblad F, Hjern A. Preterm birth and attention-deficit/hyperactivity disorder in schoolchildren. Pediatrics 2011; 127(5): 858-65.

Lips ES, Cornelisse LN, Toonen RF, Min JL, Hultman CM, International Schizophrenia C*, et al.* Functional gene group analysis identifies synaptic gene groups as risk factor for schizophrenia. Mol Psychiatry 2012; 17(10): 996-1006.

Lips ES, Kooyman M, de Leeuw C, Posthuma D. JAG: A Computational Tool to Evaluate the Role of Gene-Sets in Complex Traits. Genes 2015; 6(2): 238-51.

Ma B, Hottiger MO. Crosstalk between Wnt/beta-Catenin and NF-kappaB Signaling Pathway during Inflammation. Front Immunol 2016; 7: 378.

Marret S, Mukendi R, Gadisseux JF, Gressens P, Evrard P. Effect of ibotenate on brain development: an excitotoxic mouse model of microgyria and posthypoxic-like lesions. J Neuropathol Exp Neurol 1995; 54(3): 358-70.

Matcovitch-Natan O, Winter DR, Giladi A, Vargas Aguilar S, Spinrad A, Sarrazin S*, et al.* Microglia development follows a stepwise program to regulate brain homeostasis. Science 2016; 353(6301): aad8670.

McCarthy KD, de Vellis J. Preparation of separate astroglial and oligodendroglial cell cultures from rat cerebral tissue. J Cell Biol 1980; 85(3): 890-902.

Melief J, Koning N, Schuurman KG, Van De Garde MD, Smolders J, Hoek RM*, et al.* Phenotyping primary human microglia: tight regulation of LPS responsiveness. Glia 2012; 60(10): 1506-17.

Michell-Robinson MA, Touil H, Healy LM, Owen DR, Durafourt BA, Bar-Or A*, et al.* Roles of microglia in brain development, tissue maintenance and repair. Brain 2015; 138(Pt 5): 1138-59.

Miron VE, Boyd A, Zhao JW, Yuen TJ, Ruckh JM, Shadrach JL*, et al.* M2 microglia and macrophages drive oligodendrocyte differentiation during CNS remyelination. Nat Neurosci 2013; 16(9): 1211-8.

Miyamoto A, Wake H, Ishikawa AW, Eto K, Shibata K, Murakoshi H*, et al.* Microglia contact induces synapse formation in developing somatosensory cortex. Nat Commun 2016; 7: 12540.

Moore T, Hennessy EM, Myles J, Johnson SJ, Draper ES, Costeloe KL*, et al.* Neurological and developmental outcome in extremely preterm children born in England in 1995 and 2006: the EPICure studies. BMJ 2012; 345: e7961.

Muro S. A DNA Device that Mediates Selective Endosomal Escape and Intracellular Delivery of Drugs and Biologicals. Adv Funct Mater 2014; 24(19): 2899-906.

NCBI. SNP FAQ Archive [Internet]. Bethesda (MD): National Center for Biotechnology Information (US); 2005-. The dbSNP Mapping Process. . 2005 [cited 2018; Available from: https://www.ncbi.nlm.nih.gov/books/NBK44455/

Nosarti C, Giouroukou E, Healy E, Rifkin L, Walshe M, Reichenberg A*, et al.* Grey and white matter distribution in very preterm adolescents mediates neurodevelopmental outcome. Brain 2008; 131(Pt 1): 205-17.

Nosarti C, Nam KW, Walshe M, Murray RM, Cuddy M, Rifkin L*, et al.* Preterm birth and structural brain alterations in early adulthood. Neuroimage Clin 2014; 6: 180-91.

Opgen-Rhein R, Strimmer K. From correlation to causation networks: a simple approximate learning algorithm and its application to high-dimensional plant gene expression data. BMC systems biology 2007; 1: 37.

Pandit AS, Ball G, Edwards AD, Counsell SJ. Diffusion magnetic resonance imaging in preterm brain injury. Neuroradiology 2013; 55 Suppl 2: 65-95.

Perry VH, Nicoll JA, Holmes C. Microglia in neurodegenerative disease. Nat Rev Neurol 2010; 6(4): 193-201.

Rangon CM, Schang AL, Van Steenwinckel J, Schwendimann L, Lebon S, Fu T*, et al.* Myelination induction by a histamine H3 receptor antagonist in a mouse model of preterm white matter injury. Brain Behav Immun 2018.

Reyes-Reyes EM, Teng Y, Bates PJ. A new paradigm for aptamer therapeutic AS1411 action: uptake by macropinocytosis and its stimulation by a nucleolin-dependent mechanism. Cancer Res 2010; 70(21): 8617-29.

Riddle A, Dean J, Buser JR, Gong X, Maire J, Chen K*, et al.* Histopathological correlates of magnetic resonance imaging-defined chronic perinatal white matter injury. Ann Neurol 2011; 70(3): 493-507.

Ring DB, Johnson KW, Henriksen EJ, Nuss JM, Goff D, Kinnick TR*, et al.* Selective glycogen synthase kinase 3 inhibitors potentiate insulin activation of glucose transport and utilization in vitro and in vivo. Diabetes 2003; 52(3): 588-95.

Rivest S. Regulation of innate immune responses in the brain. Nat Rev Immunol 2009; 9(6): 429-39.

Robinson EC, Valstar M, Hammers A, Ericsson A, Edwards AD, Rueckert D. Multivariate statistical analysis of whole brain structural networks obtained using probabilistic tractography. Medical image computing and computer-assisted intervention : MICCAI International Conference on Medical Image Computing and Computer-Assisted Intervention 2008; 11(Pt 1): 486-93.

Schafer J, Strimmer K. An empirical Bayes approach to inferring large-scale gene association networks. Bioinformatics 2005; 21(6): 754-64.

Schang AL, Van Steenwinckel J, Chevenne D, Alkmark M, Hagberg H, Gressens P*, et al.* Failure of thyroid hormone treatment to prevent inflammation-induced white matter injury in the immature brain. Brain Behav Immun 2014; 37: 95-102.

Schindelin J, Arganda-Carreras I, Frise E, Kaynig V, Longair M, Pietzsch T*, et al.* Fiji: an open-source platform for biological-image analysis. Nat Methods 2012; 9(7): 676-82.

Shah DK, Doyle LW, Anderson PJ, Bear M, Daley AJ, Hunt RW*, et al.* Adverse neurodevelopment in preterm infants with postnatal sepsis or necrotizing enterocolitis is mediated by white matter abnormalities on magnetic resonance imaging at term. J Pediatr 2008; 153(2): 170-5, 5 e1.

Shi F, Yap PT, Wu G, Jia H, Gilmore JH, Lin W*, et al.* Infant brain atlases from neonates to 1- and 2-year-olds. PloS one 2011; 6(4): e18746.

Shimizu T, Kagawa T, Wada T, Muroyama Y, Takada S, Ikenaka K. Wnt signaling controls the timing of oligodendrocyte development in the spinal cord. Dev Biol 2005; 282(2): 397-410.

Shimizu T, Smits R, Ikenaka K. Microglia-induced activation of non-canonical Wnt signaling aggravates neurodegeneration in demyelinating disorders. Mol Cell Biol 2016; 36(21): 2728-41.

Shiow LR, Favrais G, Schirmer L, Schang AL, Cipriani S, Andres C*, et al.* Reactive astrocyte COX2-PGE2 production inhibits oligodendrocyte maturation in neonatal white matter injury. Glia 2017; 65(12): 2024-37.

Sieger D, Moritz C, Ziegenhals T, Prykhozhij S, Peri F. Long-range Ca2+ waves transmit brain-damage signals to microglia. Developmental cell 2012; 22(6): 1138-48.

Smith SM. Fast robust automated brain extraction. Hum Brain Mapp 2002; 17(3): 143-55.

Smyth GK. Linear models and empirical bayes methods for assessing differential expression in microarray experiments. Stat Appl Genet Mol Biol 2004; 3: Article3.

Sokol SY. Spatial and temporal aspects of Wnt signaling and planar cell polarity during vertebrate embryonic development. Semin Cell Dev Biol 2015; 42: 78-85.

Spittle AJ, Boyd RN, Inder TE, Doyle LW. Predicting motor development in very preterm infants at 12 months' corrected age: the role of qualitative magnetic resonance imaging and general movements assessments. Pediatrics 2009; 123(2): 512-7.

Spittle AJ, Walsh JM, Potter C, McInnes E, Olsen JE, Lee KJ*, et al.* Neurobehaviour at term-equivalent age and neurodevelopmental outcomes at 2 years in infants born moderate-to-late preterm. Dev Med Child Neurol 2017; 59(2): 207-15.

Squarzoni P, Oller G, Hoeffel G, Pont-Lezica L, Rostaing P, Low D*, et al.* Microglia modulate wiring of the embryonic forebrain. Cell reports 2014; 8(5): 1271-9.

Stolp BH, Fleiss B, Arai Y, Supramaniam V, Vontell R, Birtles S*, et al.* Interneuron development is disrupted in preterm brains with diffuse white matter injury: observations in mouse and human. Frontiers in physiology 2019.

Subramanian A, Tamayo P, Mootha VK, Mukherjee S, Ebert BL, Gillette MA*, et al.* Gene set enrichment analysis: a knowledge-based approach for interpreting genome-wide expression profiles. Proc Natl Acad Sci U S A 2005; 102(43): 15545-50.

Supramaniam V, Vontell R, Srinivasan L, Wyatt-Ashmead J, Hagberg H, Rutherford M. Microglia activation in the extremely preterm human brain. Pediatr Res 2013; 73(3): 301-9.

Thion MS, Ginhoux F, Garel S. Microglia and early brain development: An intimate journey. Science 2018; 362(6411): 185-9.

Tran FH, Zheng JJ. Modulating the wnt signaling pathway with small molecules. Protein science : a publication of the Protein Society 2017; 26(4): 650-61.

Twilhaar ES, Wade RM, de Kieviet JF, van Goudoever JB, van Elburg RM, Oosterlaan J. Cognitive Outcomes of Children Born Extremely or Very Preterm Since the 1990s and Associated Risk Factors A Meta-analysis and Meta-regression. Jama Pediatrics 2018; 172(4): 361-7.

van Amerongen R, Mikels A, Nusse R. Alternative wnt signaling is initiated by distinct receptors. Science signaling 2008; 1(35): re9.

van der Sar AM, Stockhammer OW, van der Laan C, Spaink HP, Bitter W, Meijer AH. MyD88 innate immune function in a zebrafish embryo infection model. Infect Immun 2006; 74(4): 2436-41.

van Haastert IC, Groenendaal F, Uiterwaal CS, Termote JU, van der Heide-Jalving M, Eijsermans MJ*, et al.* Decreasing incidence and severity of cerebral palsy in prematurely born children. J Pediatr 2011; 159(1): 86-91 e1.

Verdonk F, Roux P, Flamant P, Fiette L, Bozza FA, Simard S*, et al.* Phenotypic clustering: a novel method for microglial morphology analysis. J Neuroinflammation 2016; 13(1): 153.

Verney C, Monier A, Fallet-Bianco C, Gressens P. Early microglial colonization of the human forebrain and possible involvement in periventricular white-matter injury of preterm infants. J Anat 2010; 217(4): 436-48.

Verney C, Pogledic I, Biran V, Adle-Biassette H, Fallet-Bianco C, Gressens P. Microglial reaction in axonal crossroads is a hallmark of noncystic periventricular white matter injury in very preterm infants. J Neuropathol Exp Neurol 2012; 71(3): 251-64.

Volpe JJ. Brain injury in premature infants: a complex amalgam of destructive and developmental disturbances. Lancet neurology 2009a; 8(1): 110-24.

Volpe JJ. The encephalopathy of prematurity--brain injury and impaired brain development inextricably intertwined. Semin Pediatr Neurol 2009b; 16(4): 167-78.

Warde-Farley D, Donaldson SL, Comes O, Zuberi K, Badrawi R, Chao P*, et al.* The GeneMANIA prediction server: biological network integration for gene prioritization and predicting gene function. Nucleic Acids Res 2010; 38(Web Server issue): W214-20.

Wolf SA, Boddeke HW, Kettenmann H. Microglia in Physiology and Disease. Annu Rev Physiol 2017; 79: 619-43.

Wood NS, Marlow N, Costeloe K, Gibson AT, Wilkinson AR. Neurologic and developmental disability after extremely preterm birth. EPICure Study Group. N Engl J Med 2000; 343(6): 378-84.

Woodward LJ, Anderson PJ, Austin NC, Howard K, Inder TE. Neonatal MRI to predict neurodevelopmental outcomes in preterm infants. N Engl J Med 2006; 355(7): 685-94.

Wu HC, Shen CM, Wu YY, Yuh YS, Kua KE. Subclinical histologic chorioamnionitis and related clinical and laboratory parameters in preterm deliveries. Pediatr Neonatol 2009; 50(5): 217-21.

Yu CH, Nguyen TT, Irvine KM, Sweet MJ, Frazer IH, Blumenthal A. Recombinant Wnt3a and Wnt5a elicit macrophage cytokine production and tolerization to microbial stimulation via Toll-like receptor 4. Eur J Immunol 2014; 44(5): 1480-90.

Yuen TJ, Silbereis JC, Griveau A, Chang SM, Daneman R, Fancy SP*, et al.* Oligodendrocyte-encoded HIF function couples postnatal myelination and white matter angiogenesis. Cell 2014; 158(2): 383-96.

Zhan T, Rindtorff N, Boutros M. Wnt signaling in cancer. Oncogene 2017; 36(11): 1461-73.

Zhao C, Deng Y, Liu L, Yu K, Zhang L, Wang H*, et al.* Dual regulatory switch through interactions of Tcf7l2/Tcf4 with stage-specific partners propels oligodendroglial maturation. Nat Commun 2016; 7: 10883.

Figure legends

Figure 1. MG/Mφ are required to induce hypomyelination in our model of encephalopathy of prematurity. In (**A**) a schematic of the experimental paradigm for modelling systemic inflammation-associated encephalopathy of prematurity and the timing of analysis; MG/Mφ (microglia/macrophages) and oligodendrocytes (Oligo). Of note, experiments need to be performed between postnatal day (P1) and P5 as this is when oligodendrocyte maturation in the mouse matches that found in vulnerable preterm born infants, those born from 22-32 weeks' gestation (GA). (**B-H**) demonstration that oligodendrocyte injury in our model is dependent on activated MG/Mφ by inducing cell death in these cells. Specifically, PBS or IL-1β exposed mice were injected in the corpus callosum with vehicle (PBS) or gadolinium chloride, GdCl3; 200 nmol at P1. (**B**) Scatter plot showing the reduced numbers of pro-inflammatory (IBA1+/COX2+) and stable numbers of anti-inflammatory (IBA1+/ARG1+) MG/Mφ in corpus callosum at P3 (Mean±SEM, Mann-Whitney test, * $p<0.05$, n=3/group) as illustrated by representative images in (**C**) of IBA1-immunoreactivity (IR), COX2 -IR and Dapi (Scale bar: 100μm). Following GdCl3 treatment, representative images showing MBP-IR (**D**) and OLIG2- IR (**E**) (scale bars: 20μm) in the corpus callosum at P15, and min to max box and whiskers plots of the quantification of MBP-IR (**F**) and OLIG2-IR (**G**) (Mann–Whitney test, * $p<0.05$, n=5- 6/group). The requirement for the presence of MG/Mφ to illicit demyelination was also verified in vitro in mixed glial cultures in (**H**), scatter plots of MBP-IR normalized by OLIG2+ cell number in mixed cell culture (Mean, Mann-Whitney test ** $p<0.01$ and n =18/group).

Figure 2. MG/Mφ have a subtly altered morphology and bi-phase alterations to phenotype in our model of encephalopathy of prematurity. Quantification in (**A**) of the complexity of MG/Mφ ramifications and process length in CX3CR1$^{GFP/+}$ mice exposed via i.p. injection to PBS or IL-1β for 3 hours (P1) or for 48 hours (P3). The proportion (%) and the scatter plots of the complexity index and the process length MG/Mφ (Mean, Mann-Whitney test, * $p<0.05$, n=4/group). (**B**) Representative images of IL-1β induced decrease in the complexity index in GFP+ MG/Mφ at P3 (Scale bar: 25μm). **(C)** MG/Mφ phenotype over time is represented by min to max box and whiskers plots of pro-inflammatory, anti-inflammatory and immuno-regulatory markers levels by RT-qPCR in CD11B+ MG/Mφ from brain in PBS or IL-1β injected mice. See also **Supp Figure 1, Supp Figure 2 and Supp Table 5**. mRNA levels are presented as a fold change relative to PBS group. (Two-way ANOVA with post hoc

Bonferroni's test ,* p<0.05, ** p<0.01, *** p<0.001, n/group is indicated on the figure under the legend).

Figure 3. The Wnt pathway is down-regulated in pro-inflammatory MG and modulates MG activation in vitro. (**A**) Transcriptomic data reveals that the Wnt signalling pathway is strongly associated with MG/Mφ activation in our model and (**B**) builds a cohesive network of multi-modal interactions between Wnt pathway genes in the MG/Mφ co-expression network. (**C**) Validation of a selection of Wnt targets from the array data showing min to max box and whiskers plots of mRNA level presented as a fold change relative to PBS group by RT-qPCR in CD11B+ MG/Mφ from PBS or IL-1β-exposed mice. See also **Supp Figure 3**. Two-way ANOVA, post hoc Bonferroni's test, * p<0.05, ** p<0.01 *** p<0.001, n/group is indicated on the graph). (**D**) Scatter plot of β-catenin protein level from ELISA in CD11B+ MG/Mφ from PBS or IL-1β-exposed mice at P3. Data are expressed as fold change relative to PBS group, (Mean±SEM, Student's t-test, * p<0.05, n=9/group). In **(E)** β-catenin pathway inhibition, with XAV939, induced a pro-inflammatory like activation in primary microglia. Min to max box and whiskers plots of mRNA levels are presented as a fold change relative to vehicle group. (Student's t-test, * p<0.05, ** p<0.01, n=12/group). In (**F**) β-catenin pathway activation induced by blocking Axin2 with siRNA (see also **Supp Figure 3I,** approx. 45% Axin2 mRNA decrease**)** and in (**G**) inhibition of GSK3β, a β-catenin inhibitor, with CT99021 reduced primary microglia activation induced by IL-1β. Min to max box and whiskers plots of mRNA levels presented as a fold change relative to vehicle group. (One-way ANOVA with post hoc Newman-Keuls's test. Effects of IL-1β on gene expression are shown with + p<0.05, ++ p<0.01, +++p<0.001; effects of Axin2 siRNA or CT99021 to alter the IL-1β effects are shown with * p<0.05, ** p<0.01, ***p<0.001, n =6/group). In (**H**) Effects of modulating Wnt with XAV939, Axin2 siRNA and CT99021 on phosphorylation of β-catenin (PSer45 β-catenin/β-catenin ratio) in primary microglia. (Scatter plots, Mean±SEM, Mann-Whitney test * p<0.05, n=3/group).

Figure 4. Wnt/β-catenin pathway regulates MG/Mφ activation and hypomyelination in vivo. Wnt signalling was modulated in vivo with pharmacological techniques in zebrafish (**A-C**) and mice (**D**) and using gene knockout in mice (**E-G**). In (**A**) location of LPS microinjection (5ng/injection) into the zebrafish hindbrain at 72 hpf in pu1::Gal4-UAS::TagRFP morpholinos

followed by analysis at 120 hpf. In (**B**) a scatter plot of quantification of RFP labelled MG and in (**C**) representative images of RFP MG in these zebrafish brains after LPS injection in the presence or not in their growth solution of Wnt/β-catenin pathway activators LiCl (80mM) and CT99021 (3μM) or Wnt inhibitor XAV939 (5μM). (Mean±SEM, One-way ANOVA with post hoc Newman-Keuls's test, ** $p<0.01$, ***$p<0.001$). Scale bar: 40μm. In (**D**) analysis of the phenotype of CD11B+ cell isolated from P1 mice injected i.c.v. with XAV939 (0.5 nmol) alone (no i.p. IL-1β), demonstrating increased MG/Mφ activation with Wnt agonism. Min to max box and whiskers plots of quantification of Nos2, Ptgs2, Tnfα, Il1rn, Socs3 and Il4ra mRNA by RT-qPCR. mRNA levels are presented as a fold change relative to PBS/DMSO group. (Student's t-test, * $p<0.05$, ** $p<0.01$ and ***$p<0.001$ n=7-10/group). In (**E,F**) β-catenin deficit in MG driven by β-catenin$^{flox/+}$/LysM$^{Cre/+}$ (β-catenin$^{\Delta/+}$) induces hypomyelination. Scatter plots of quantification by RT-qPCR of (**E**) *Ctnnb1* mRNA deficit in CD11B+ MG/Mφ from P10 β-catenin$^{\Delta/+}$ mice (n=6-12/group) and in (**F**) *Mbp* mRNA deficit in the anterior brain at P10 in β- catenin$^{\Delta/+}$ mice. mRNA levels are presented as a fold change relative to control (Ctrl) mice (β- catenin$^{+/+}$/LysM$^{Cre/+}$) (n=4/group) (Mean, Mann-Whitney test, * $p<0.05$, *** $p<0.01$). In (**H**) min to max box and whiskers plot of grey density level of MBP immunoreactivity (MBP-IR) in the corpus callosum and cingulum at P30 relative to Ctrl mice. (Mann-Whitney test, * $p<0.05$, n=6/group and illustrated by representative images of MBP-IR in (**G**). (Scale bar: 40μm)

Figure 5: Human MG activation leads to Wnt/β-catenin down-regulation and genetic variation in the Wnt pathway associates with preterm infant white matter phenotype

In (**A**) human primary MG exposed to LPS showing immunoreactive changes with IBA1 (scale bar = 50μm), and (**B**) up-regulated mRNA expression for COX2 (*PTGS2*) and (**C**) the associated decrease in the expression of the gene for β-catenin (*CTNNB1*)**,** (Min to max box and whiskers plots, Student's t-test, **$p<0.01$, ***$p<0.0001$, n=6-9/group). In (**D**) a schematic of the analysis for any association between SNPs in the WNT pathway and the preterm infant white matter phenotype. Common genetic variation (SNPs) in the WNT gene-set were enriched for variants associated with tractography features when compared to random matched gene-sets, i.e., competitive test, $p=0.037$, 1000 permutations, (**E, blue inset**) and is also associated with white matter probabilistic tractography in preterm infants, compared with the null

background, i.e., self-contained test, p=0.064, 1000 permutations (**E, blue inset**). In (**F**) is the predicted consequences of all of the SNPs found in the top 10 ranked WNT genes shown in **Table 1**, a total of 42 SNPs. In (**G**) the relationships between these ten genes significantly associated with the tractography phenotype is reconstructed in a high confidence interaction network specific to the human brain, retrieved from known tissue-specific expression and regulatory data (Greene et al., 2015).

Figure 6. Nanocarrier delivery of a Wnt/β-catenin pathway activator L803mts regulates MG/Mφ activation in our encephalopathy of prematurity model. In (**A**) representative images of the *in vivo* uptake of 3DNA by IBA1+ cells in the subventricular white matter 4 hours after i.c.v. administration of 3DNA SCR Cy3 (control) or 3DNA L803mts Cy3 (200ng), scale bar: 40μm. Plus orthogonal view of white box inset showing co-localisation in detail, scale bar: 10μm. See also **Supp Figure 4A,B, Supp Figure 5,** and **Supp Video 1**. In (**B**) min to max box and whiskers plots of *Nos2, Ptgs2, Tnfα, Il1rn, Socs3* and *Il4ra* mRNA by qRT-PCR in CD11B+ MG/Mφ cells from i.c.v. injected PBS or IL-1β-treated mice with of 3DNA SCR Cy3 or 3DNA L803mt. mRNA levels are presented as a fold change relative to vehicle group (One-way ANOVA with post hoc Newman-Keuls's test, ++ $p<0.01$, +++ $p<0.001$ for statistically significant difference between the PBS and IL-1β groups also exposed to 3DNA SCR Cy3. * $p<0.05$, ** $p<0.01$ for the effects of 3DNA Wnt modulator delivery, n=5-6 for PBS groups and 9 for IL-1β- groups).

Figure 7. Nanocarrier delivery of a Wnt/β-catenin pathway activator L803mts in microglia reduces IL-1β-induced hypomyelination and memory deficit. In (**A**) representative images of *in vivo* uptake of 3DNA by IBA1+ cells in subventricular white matter at P5 after i.p. injections of 3DNA L803mts Cy3 or 3DNA SCR Cy3 (500ng/injection). Scale bar: 40μm. In (**B**) min to max box and whiskers plot of *Mbp* mRNA by qRT-PCR in the anterior brain of mice at P10. mRNA levels are presented as a fold change relative to 3DNA SCR Cy3/PBS group (One way-ANOVA with Newman-Keuls's test, * $p<0.05$, ** $p<0.01$, n=9-12/group). See also **Supp Figure 5C,D.** In (**C**) a representative image of ACTIN and MBP immuno-blot and (**D**) the min to max box and whiskers plots of quantification of the four isoforms of MBP in the anterior brain of mice at P15. Protein levels were normalised to ACTIN and are presented as a fold change relative to 3DNA SCR Cy3/PBS group (One way-ANOVA with Newman-Keuls's test, * $p<0.05$, *** $p<0.001$, ** $p<0.01$, n=6-8/group). In (**E**) a representative image of electron microscope (EM) image of the corpus callosum from mice at

P30. In (**F**) the violin plots of the G-ratios from the EM analysis showing improvements in the Wnt agonist group, 3DNA L803mts (Kruskall-Wallis test, ***p<0001 n=4-5/group). Microglial targeted Wnt agonism also induced functional improvements. In (G) data from trials of the Barnes maze for spatial learning and in (H) short-term memory retention and (**I)** long-term memory retention **(I**) in 3-month-old mice. See also **Supp Figure 6**. Memory retention present in the 30 second trial period on day 5 of the test (probe trial, in **H**) was measured by recording of the distance travelled in the target sextant (Min to max box and whiskers plot, univariate t test * p<0.05 n=10/group). In (**I**) the long-term memory deficits was measured via the distance travelled to reach the target on the 15th day after the start of testing (Min to max box and whiskers plot, one-way ANOVA with Bonferroni post hoc was used ** p<0.01. n= 9/group).

Table 1: Functional descriptions of the ten genes within the WNT gene-set containing SNPs that were most significantly associated with the preterm infant tractography phenotype outlined in Figure 5D-E. The predicted consequences of changes in these genes in found in Figure 5F.

Supplementary figures

Supplementary Figure 1 related to Figure 2. Expression of phenotype markers by MG/Mφ in IL-1β treated mice at P3. (A) Min to max box and whisker of the number of CD16+, CD68+/iNOS+, CD68+/COX2+, CD68+/ARG1+ and MR + (CD206) cells at P3 from PBS and IL-1β treated mice. Data are expressed as the number of positive cells per field (Mann-Whitney test,* $p<0.05$ and **$p<0.01$, n=7-8/group). Representative images at P3 in the corpus callosum of the effect of IL-1β on the number of **(B)** CD68+/iNOS+ and CD68+/ARG1+ cells **(C)** CD68+/COX2+ and **(D)** CD16+ and MR+ cells. Scale bar: 50μm

Supplementary Figure 2 related to Figure 3 and Supp Table 5. Properties of the networks formed from the transcriptomic analysis of MG and oligodendrocytes following exposure to IL-1β. In (**A**) the structural properties of the transcriptomic network from the microarray analysis performed on CD11B+ and O4+ cell fractions isolated by MACS. Reconstructed gene networks by cell type and condition, local FDR <1% (OG: oligodendrocytes; MG MG/Mφ; PBS: control). (**B**) Visual representation of the output of transcriptomic analysis of MG and oligodendrocytes following exposure to IL-1β. Under control conditions (PBS) the OG co-expression network appears less dense, structured with interconnected clusters (34 connected components) where most genes are not direct neighbours of one another (characteristic path length 5.5). With exposure to IL-1β there is a noticeable change in the OG network structure, so that there are many more genes being co-expressed (an increase from 571 nodes, 1229 edges in PBS to 1583 nodes, 6457 edges in IL-1β) and they are more highly interconnected (characteristic path length 2.9). The control (PBS) MG co-expression network is also relatively clustered and less dense, and on exposure to IL-1β there is a dramatic increase in co-expression (786 nodes, 1810 edges in PBS to 3113 nodes and 48104 edges in IL-1β). This demonstrates that at rest MG are more transcriptionally active than OG, and both cell-types respond strikingly to IL-1β exposure with a global activation of gene expression that is particularly pronounced for MG.

Supplementary Figure 3 related to Figure 4. Validation in primary MG of an inverse relationship between pro-inflammatory status and the Wnt/β-catenin pathway. In **(A)** MG phenotypes under 4hours of IL-1β or LPS stimulation were assessed via pro-inflammatory markers anti-inflammatory markers and immuno-regulator markers by RT-qPCR. mRNA levels are presented as a fold change relative to PBS exposed MG. Data are expressed as

mean±SEM, n in the brackets (Student's t-test, * p<0.05, ** p<0.01 and ***P<0.001). **(B)** MG phenotype induced after 4 hours of exposure to IL-1β in primary MG as assessed with immunoreactivity (IR) for COX2 (pro-inflammatory) ARG1 (anti-inflammatory) and IL1RA (immuno-regulator). Scale bar: 50µm. Canonical Wnt pathway expression in primary MG as altered by **(C)** 4 hours of IL-1β exposure as assessed by RT-qPCR for *Ctnnb1, Tcf1, Lef, Axin1, Axin2* and Wnt receptors Frizzled (*Fzd*) *3,4,6* mRNA, (**D**) 4 hours of LPS exposure as assessed by RT-qPCR for *Ctnnb1, Tcf1, Lef, Axin1 and Axin2* mRNA, **(E)** 4 hours of IL-4 exposure as assessed by RT-qPCR for *Ctnnb1, Tcf1, Lef, Axin1 and Axin2* mRNA. Min to max box and whisker of mRNA levels presented as a fold change relative to control (PBS treated) MG. (Min to max box and whisker, Student's t-test: * p<0.05, ** p<0.01 and *** p<0.001, n on the figure). **(F)** IL-1β induces down-regulation of β-catenin immunoreactivity in primary MG after 4 hours of stimulation. Scale bar: 50µm. **(E)** IL-1β induces down-regulation of total β-catenin without any modification of the PSer45 β-catenin/β-catenin ratio as assessed via ELISA (normalized to PBS control) in primary MG after 4 hours of stimulation. (Min to max box and whisker, Student t-test** p<0.01, n=14/group). **(G)** IL-4 induces down-regulation of Pser45 β-catenin/β-catenin ratio without any modification of total β-catenin in primary MG as assessed with ELISA after 4 hours of stimulation. (Min to max box and whisker Student's t-test, * p<0.05, n=7/group). (**H**) Min to max box and whisker of *Axin2* mRNA level in primary MG transfected with Axin2 siRNA presented as a fold change relative to control (negative control siRNA) (Student's t-test: *** p<0.001, n=14-15/group)

Supplementary Figure 4. Non-canonical Wnt pathway blockade has no effect on the activation of primary MG stimulated by IL-1β. Inhibition of Protein Kinase C by Chelerythrine has no effect on MG activation. Min to max box and whisker of *Nos2, Ptgs2, Il1rn* and *Socs3* mRNA level by RT-qPCR in control (PBS) and IL-1β treated primary MG with Chelerythrine (1 or 3µM) or DMSO. mRNA levels are presented as a fold change relative to control/DMSO group. (# p<0.05, ## p<0.01, showed significant difference between PBS/DMSO and IL-1β/DMSO groups. Kruskal-Wallis test with Dunns *post-hoc* test, n=3/group)

Supplementary Figure 5 related to Figure 6. Cell and organ specific analysis of the uptake by MG of 3DNA Cy3 labelled nanoparticles. (A) 3DNA uptake by IBA-1+ cells in mixed primary cultures of astrocytes, OPCs and MG after incubation with 3DNA Cy3 (200ng/ml) for

24 hours. Scale bar: 40µm. **(B)** 3DNA uptake by a primary MG following incubation with 3DNA L803mts Cy3 (200ng/ml) for 5 hours. Scale bar: 10µm. Representative images of the undetectable uptake of 3DNA by the **(C)** spleen and **(D)** the liver. Scale bar: 100µm

Supplementary Figure 6. Nanocarrier-mediated delivery of a Wnt/β-catenin pathway activator L803mts regulates MG/Mφ activation in primary MG. In (**A**) representative images of the *in vitro* uptake of 3DNA by primary MG 4 hours after 3DNA L803mts Cy3 exposure. In (**B**) effects of 3DNA L803mts Cy3 exposure to reduce the IL-1β-induced MG/Mφ activation as evaluated by qRT-PCR quantification of *Nos2, Ptgs2, Tnfα, Il1rn, Socs3* and *Il4ra* mRNA. mRNA levels are presented as a fold change relative to 3DNA SCR Cy3/PBS group (Min to max box and whisker, one-way ANOVA with *post hoc* Newman-Keuls's test: ++ $p<0.01$, +++$p<0.001$ indicate a statistically significant difference between the PBS and the IL-1β groups also exposed to 3DNA SCR Cy3. For the effects of Wnt modulator delivery, * $p<0.05$, ** $p<0.01$, n=5/group).

Supplementary Figure 7. Nanocarrier-mediated delivery of a Wnt/β-catenin pathway activator L803mts has no effect on indices of basal behaviour in our encephalopathy of prematurity model. (**A**) ACTIN and MBP immuno-blot from mice anterior cortex at P15. (**B**) Actimetry data including horizontal locomotion and rearing over a 24 hour period, mean±SEM n=10/group. In (**C**) data on distance travelled and time spent inactive in the Open Field test (Min to max box and whisker n=10/group)

Supplementary tables: All available as individual tabs within one Excel spreadsheet

Supp Table 1. *List of the numbers of independent and total experimental replicates presented in each figure.*

Supp Table 2*. List of primer sequences*

Supp Table 3. *Biological pathway analysis using the Broad Institute MsigDB database for each of the four conditions. Of note for MG exposed to IL-1β Wnt signalling is highly significantly enriched.*

Supp Table 4. *Clinical variables of the cohort described in the imaging-genomics analysis*

Supp Table 5. *Genes found within the co-expression networks for each of the four GGM outputs. See also, Supp Figure 1.*

Supp Table 6. *GSEA including genes down-regulated in the array analysis, showing a predominance of Wnt enrichment in the down-regulated genes.*

Supp Table 7. *Analysis of the 10 highly ranked genes showing statistical outputs in full for an association with the white matter connectivity phenotype.*

Supp Table 8*. Genes creating a coherent interaction network built around the 10 WNT pathway genes with SNPs highly associated with the preterm white matter connectivity phenotype.*

Supp Table 9. *Details for each of the 42 SNPs for analysis from the 10 genes most highly associated with the preterm white matter phenotype*

Supp Table 10*. Consequences predicted for the 42 SNPs found in the 10 genes of high relevance to the preterm white matter connectivity phenotype. Summary of effects found in Figure 5F.*

Supplementary video

Video 1: *Staining in the periventricular white matter for IBA1 (green) and visible 3DNA with Cy3 tag (red). Tissue collected 4 hours after a single IL1β and 3DNA i.p. injection at P1.*

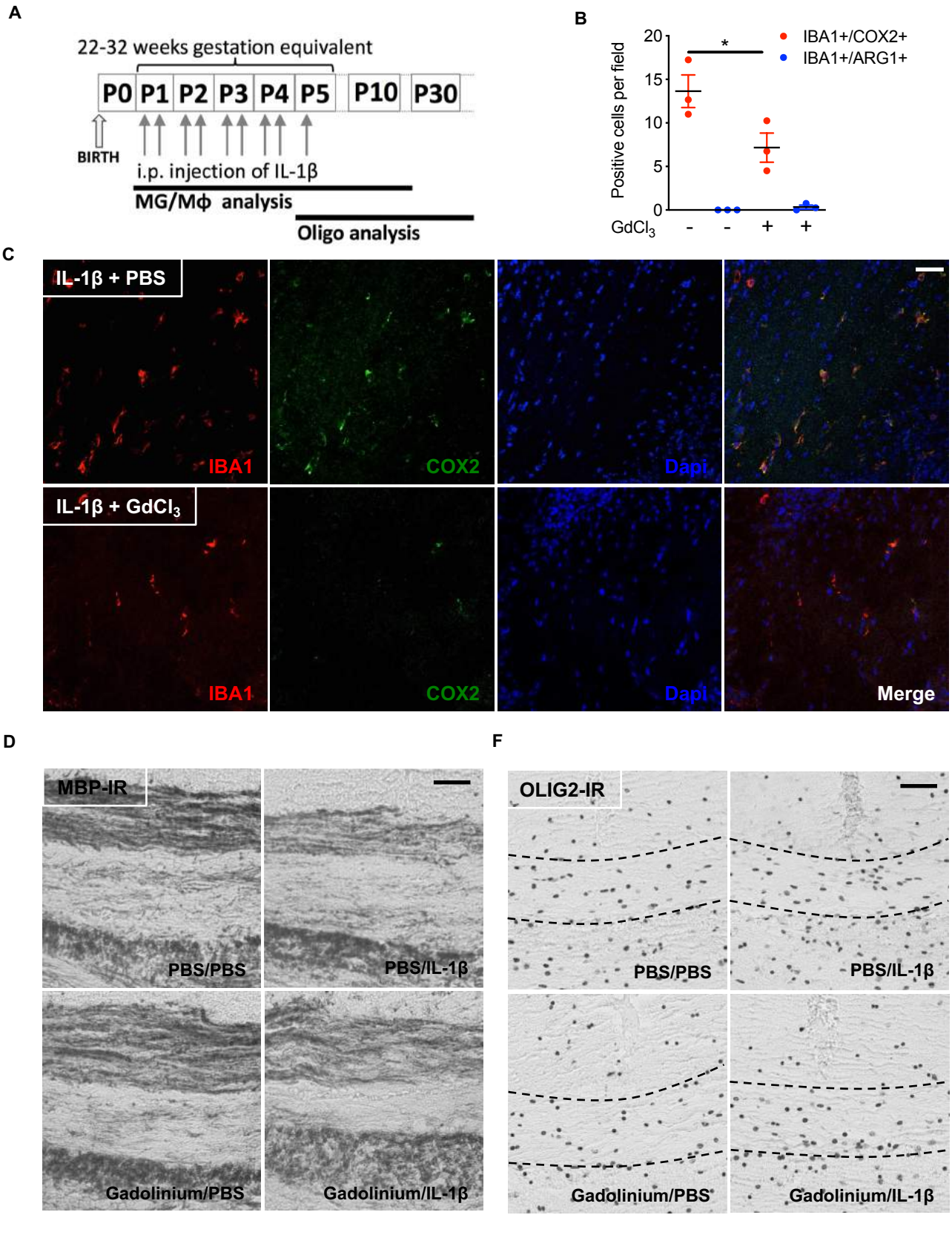
A
22-32 weeks gestation equivalent
P0 P1 P2 P3 P4 P5 P10 P30
BIRTH
i.p. injection of IL-1β
MG/Mϕ analysis
Oligo analysis
B
Positive cells per field
IBA1+/COX2+
IBA1+/ARG1+
GdCl3
C
IL-1β + PBS
IL-1β + GdCl3
IBA1
COX2
Dapi
Merge
D
MBP-IR
PBS/PBS
PBS/IL-1β
Gadolinium/PBS
Gadolinium/IL-1β
F
OLIG2-IR
E
MBP-IR Quantification
PBS
IL-1β
G
OLIG2-IR Quantification
n.s.
H
Mixed glial culture
MBP-IR IR area/OLIG2 cells number (Normalized data)

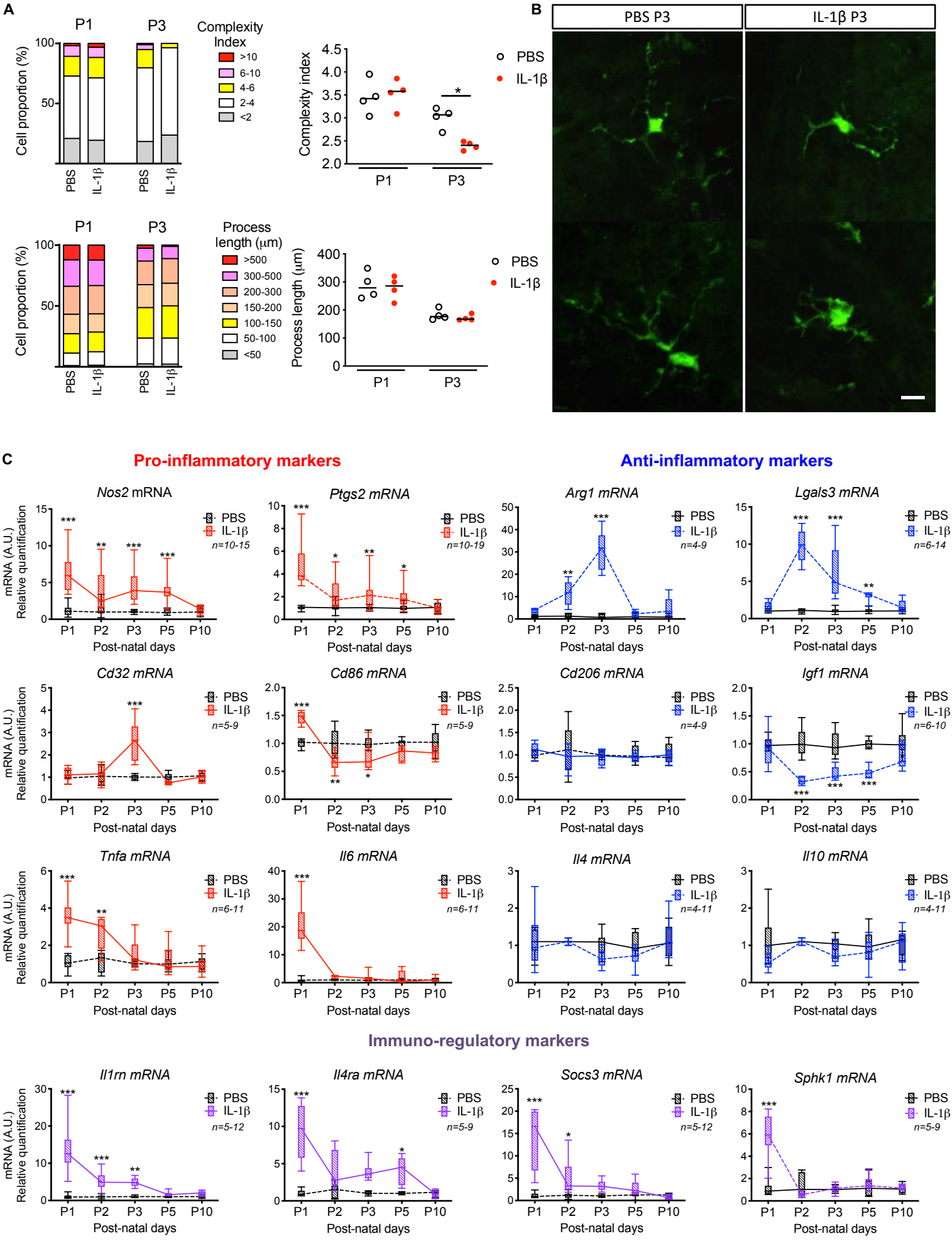
A
P1
P3
Complexity Index
>10
6-10
4-6
2-4
<2
Cell proportion (%)
PBS
IL-1β
Complexity index
Process length (μm)
>500
300-500
200-300
150-200
100-150
50-100
<50
Process length (μm)
B
PBS P3
IL-1β P3
C
Pro-inflammatory markers
Anti-inflammatory markers
Immuno-regulatory markers
Nos2 mRNA
Ptgs2 mRNA
Arg1 mRNA
Lgals3 mRNA
Cd32 mRNA
Cd86 mRNA
Cd206 mRNA
Igf1 mRNA
Tnfa mRNA
Il6 mRNA
Il4 mRNA
Il10 mRNA
Il1rn mRNA
Il4ra mRNA
Socs3 mRNA
Sphk1 mRNA
mRNA (A.U.) Relative quantification
Post-natal days
n=10-15
n=10-19
n=4-9
n=6-14
n=5-9
n=5-9
n=4-9
n=6-10
n=6-11
n=6-11
n=4-11
n=4-11
n=5-12
n=5-9
n=5-12
n=5-9

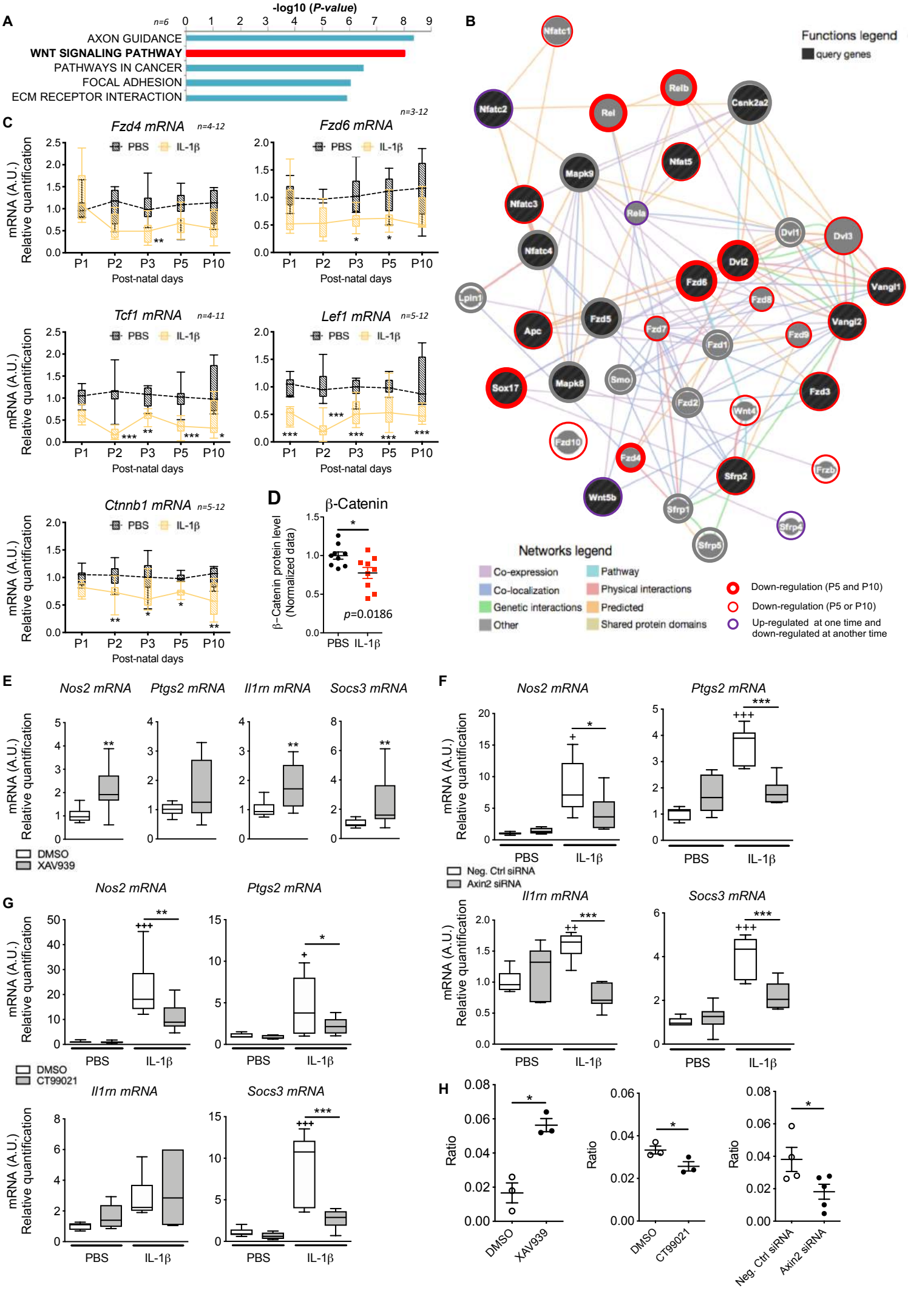
A
-log10 (P-value)
n=6
AXON GUIDANCE
WNT SIGNALING PATHWAY
PATHWAYS IN CANCER
FOCAL ADHESION
ECM RECEPTOR INTERACTION
B
Functions legend
query genes
Networks legend
Co-expression
Co-localization
Genetic interactions
Other
Pathway
Physical interactions
Predicted
Shared protein domains
Down-regulation (P5 and P10)
Down-regulation (P5 or P10)
Up-regulated at one time and down-regulated at another time
C
Fzd4 mRNA
Fzd6 mRNA
Tcf1 mRNA
Lef1 mRNA
Ctnnb1 mRNA
PBS
IL-1β
mRNA (A.U.) Relative quantification
Post-natal days
D
β-Catenin
β-Catenin protein level (Normalized data)
p=0.0186
E
Nos2 mRNA
Ptgs2 mRNA
Il1rn mRNA
Socs3 mRNA
DMSO
XAV939
F
Neg. Ctrl siRNA
Axin2 siRNA
G
DMSO
CT99021
H
Ratio
DMSO
XAV939
CT99021
Neg. Ctrl siRNA
Axin2 siRNA

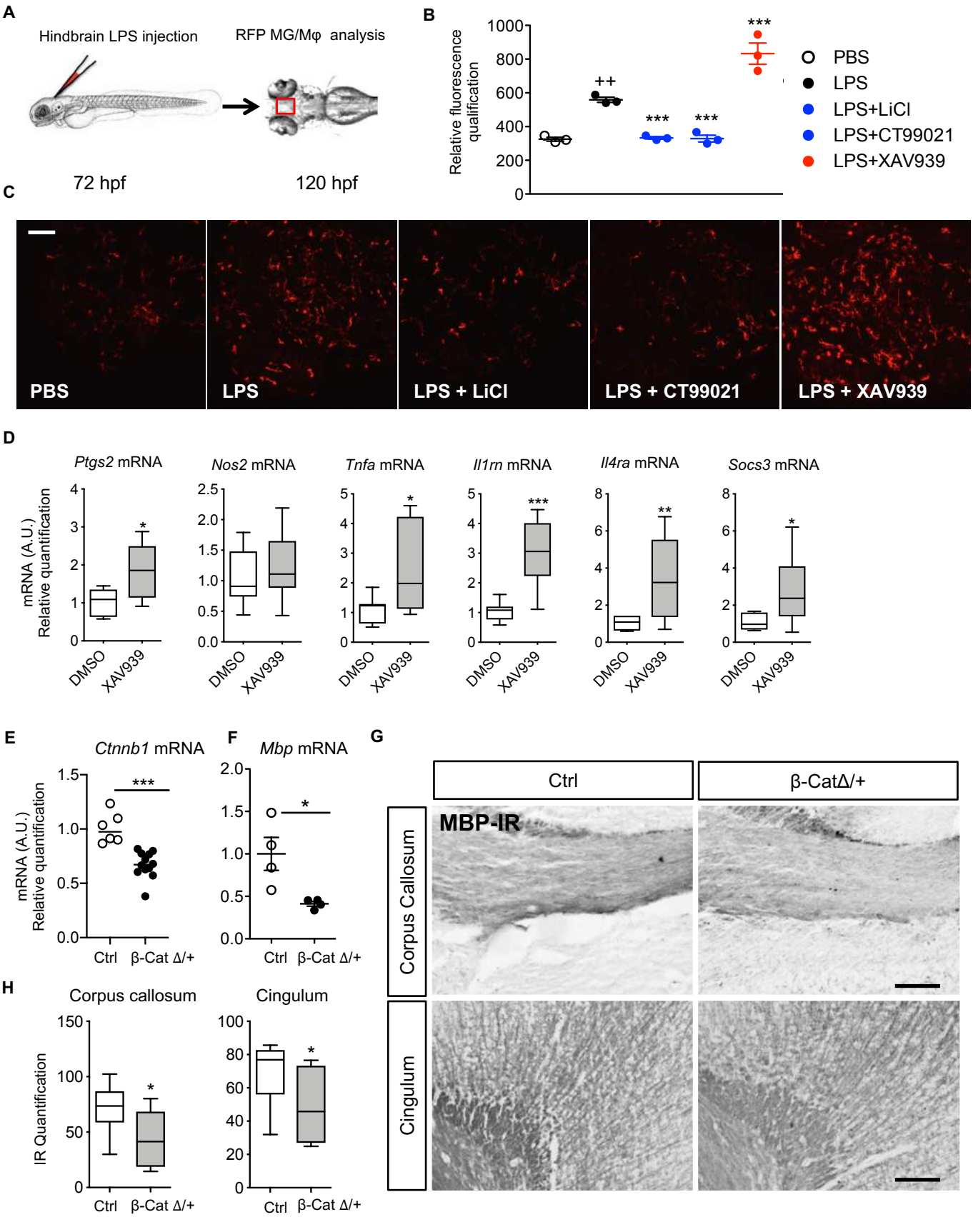
A
Hindbrain LPS injection
RFP MG/Mφ analysis
72 hpf
120 hpf
B
Relative fluorescence qualification
1000
800
600
400
200
0
++
***
***
***
PBS
LPS
LPS+LiCl
LPS+CT99021
LPS+XAV939
C
PBS
LPS
LPS + LiCl
LPS + CT99021
LPS + XAV939
D
Ptgs2 mRNA
Nos2 mRNA
Tnfa mRNA
Il1rn mRNA
Il4ra mRNA
Socs3 mRNA
mRNA (A.U.)
Relative quantification
DMSO
XAV939
E
Ctnnb1 mRNA
mRNA (A.U.)
Relative quantification
Ctrl
β-Cat Δ/+
F
Mbp mRNA
G
Ctrl
β-CatΔ/+
MBP-IR
Corpus Callosum
Cingulum
H
Corpus callosum
Cingulum
IR Quantification

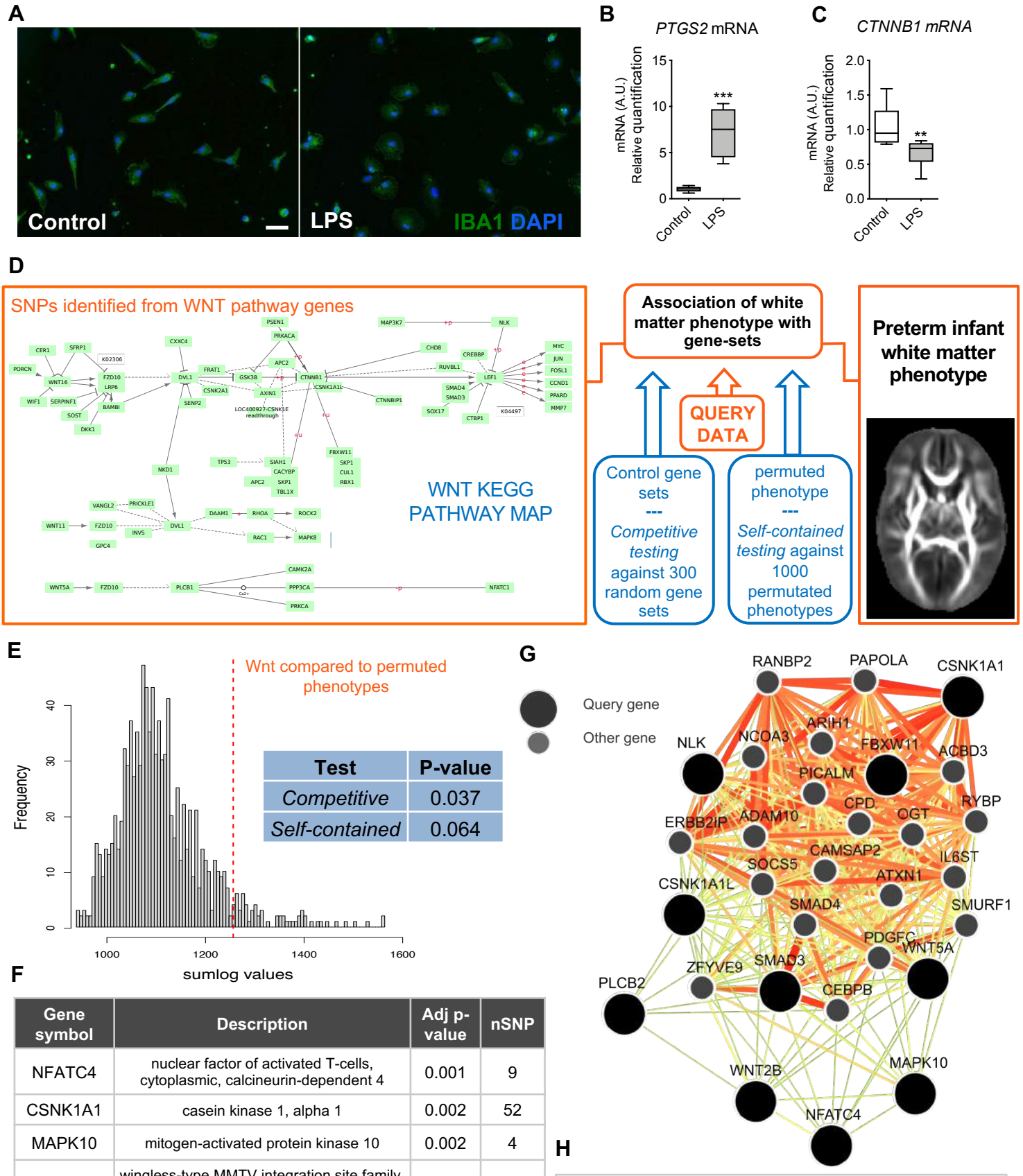
A
Control
LPS
IBA1 DAPI
B
PTGS2 mRNA
mRNA (A.U.)
Relative quantification
***
Control
LPS
C
CTNNB1 mRNA
mRNA (A.U.)
Relative quantification
**
Control
LPS
D
SNPs identified from WNT pathway genes
WNT KEGG
PATHWAY MAP
Association of white matter phenotype with gene-sets
QUERY DATA
Control gene sets

Competitive testing against 300 random gene sets
permuted phenotype

Self-contained testing against 1000 permutated phenotypes
Preterm infant white matter phenotype
E
Wnt compared to permuted phenotypes
Frequency
sumlog values
Test
P-value
Competitive
0.037
Self-contained
0.064
G
Query gene
Other gene
RANBP2
PAPOLA
CSNK1A1
NLK
NCOA3
ARIH1
FBXW11
ACBD3
PICALM
CPD
RYBP
ERBB2IP
ADAM10
OGT
CAMSAP2
IL6ST
SOCS5
ATXN1
CSNK1A1L
SMAD4
SMURF1
PDGFC
WNT5A
ZFYVE9
SMAD3
PLCB2
CEBPB
WNT2B
MAPK10
NFATC4
F
Gene symbol
Description
Adj p-value
nSNP
NFATC4
nuclear factor of activated T-cells, cytoplasmic, calcineurin-dependent 4
0.001
9
CSNK1A1
casein kinase 1, alpha 1
0.002
52
MAPK10
mitogen-activated protein kinase 10
0.002
4
WNT2B
wingless-type MMTV integration site family, member 2B
0.007
6
SMAD3
SMAD family member 3
0.014
57
FBXW11
F-box and WD repeat domain containing 11
0.015
4
WNT5A
wingless-type MMTV integration site family, member 5A
0.023
12
NLK
nemo-like kinase
0.026
11
CSNK1A1L
casein kinase 1, alpha 1-like
0.033
11
PLCB2
phospholipase C, beta 2
0.038
5
H
Predicted consequences of SNPs
intron_variant: 70%
non_coding_transcript_variant: 10%
NMD_transcript_variant: 5%
downstream_gene_variant: 4%
synonymous_variant: 4%
3_prime_UTR_variant: 3%
regulatory_region_variant: 2%
upstream_gene_variant: 2%
non_coding_transcript_exon_variant
Others

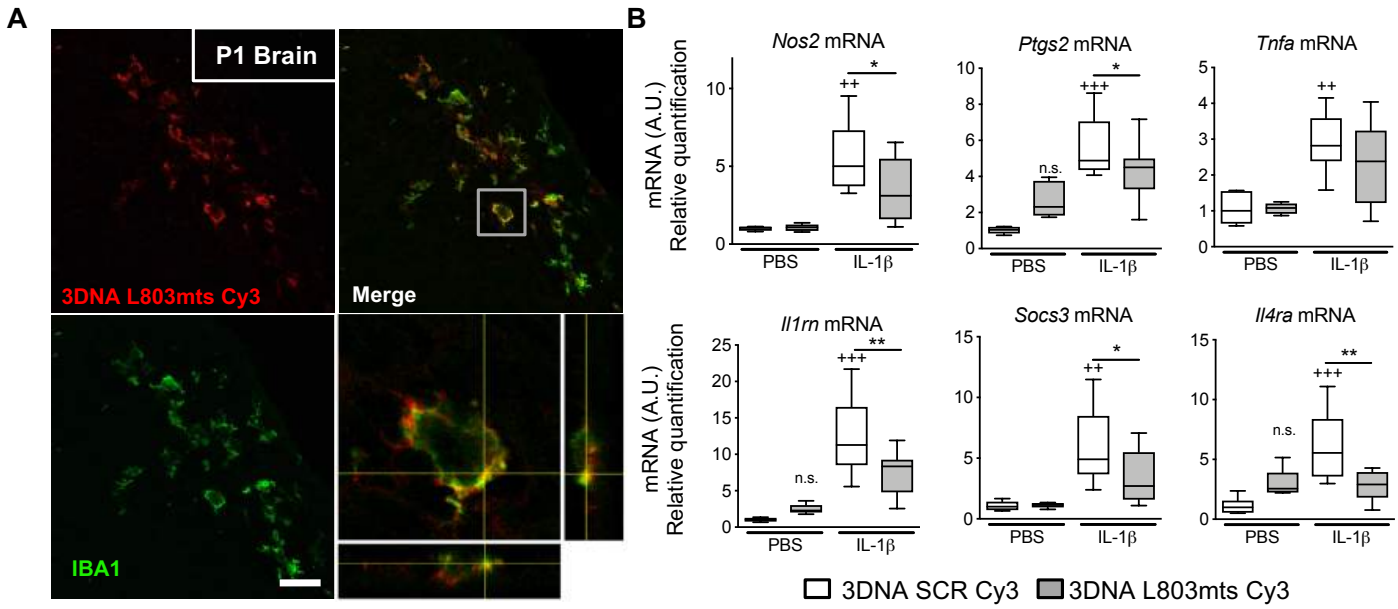
A
P1 Brain
3DNA L803mts Cy3
Merge
IBA1
B
Nos2 mRNA
Ptgs2 mRNA
Tnfa mRNA
Il1rn mRNA
Socs3 mRNA
Il4ra mRNA
mRNA (A.U.)
Relative quantification
PBS
IL-1β
n.s.
3DNA SCR Cy3
3DNA L803mts Cy3

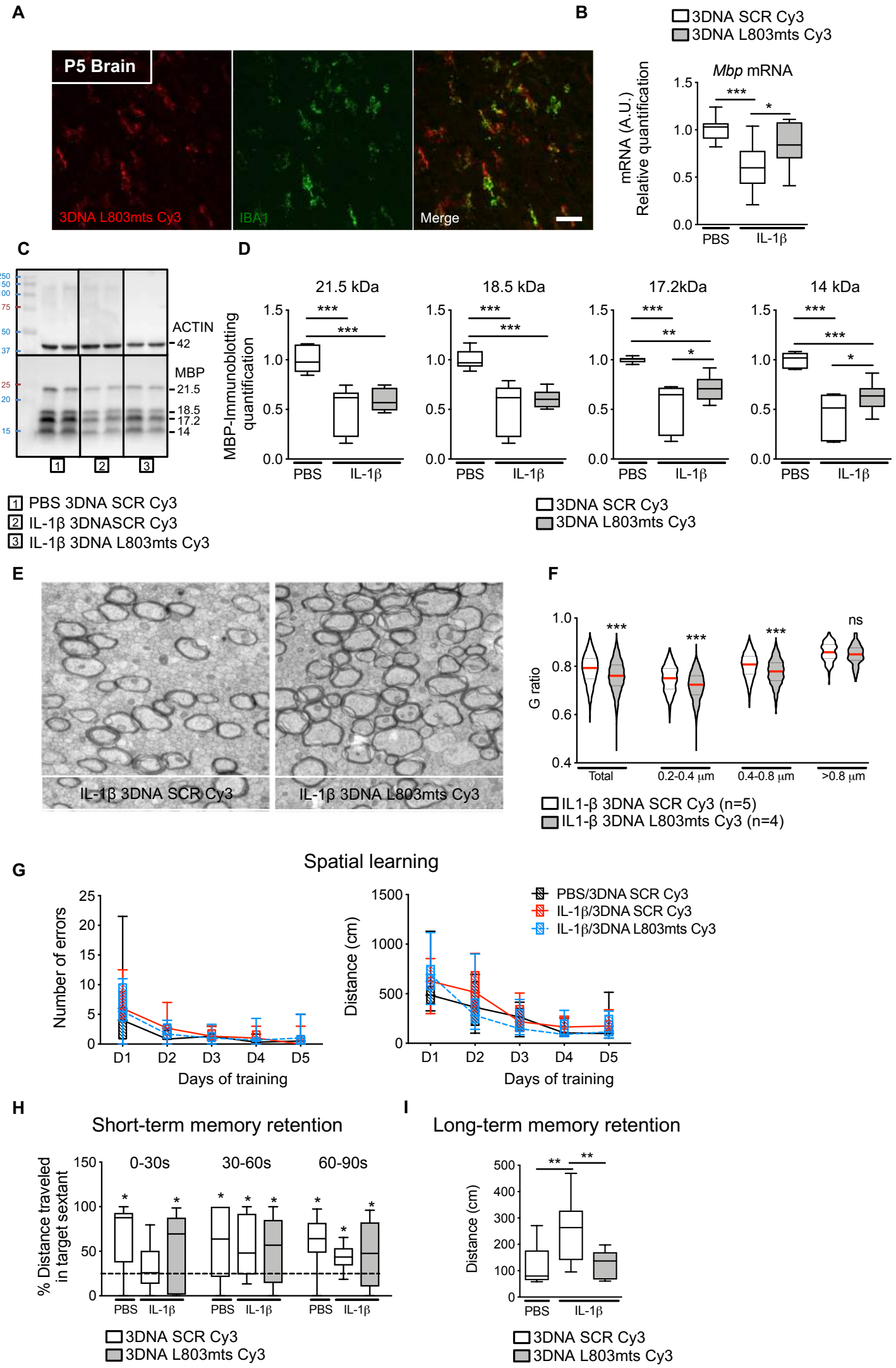
A
P5 Brain
3DNA L803mts Cy3
IBA1
Merge
B
3DNA SCR Cy3
3DNA L803mts Cy3
Mbp mRNA
mRNA (A.U.)
Relative quantification
PBS
IL-1β
C
ACTIN
42
MBP
21.5
18.5
17.2
14
1 PBS 3DNA SCR Cy3
2 IL-1β 3DNASCR Cy3
3 IL-1β 3DNA L803mts Cy3
D
21.5 kDa
18.5 kDa
17.2kDa
14 kDa
MBP-Immunoblotting quantification
3DNA SCR Cy3
3DNA L803mts Cy3
E
IL-1β 3DNA SCR Cy3
IL-1β 3DNA L803mts Cy3
F
G ratio
Total
0.2-0.4 µm
0.4-0.8 µm
>0.8 µm
ns
IL1-β 3DNA SCR Cy3 (n=5)
IL1-β 3DNA L803mts Cy3 (n=4)
G
Spatial learning
Number of errors
Distance (cm)
Days of training
PBS/3DNA SCR Cy3
IL-1β/3DNA SCR Cy3
IL-1β/3DNA L803mts Cy3
H
Short-term memory retention
% Distance traveled in target sextant
0-30s
30-60s
60-90s
3DNA SCR Cy3
3DNA L803mts Cy3
I
Long-term memory retention
Distance (cm)
3DNA SCR Cy3
3DNA L803mts Cy3

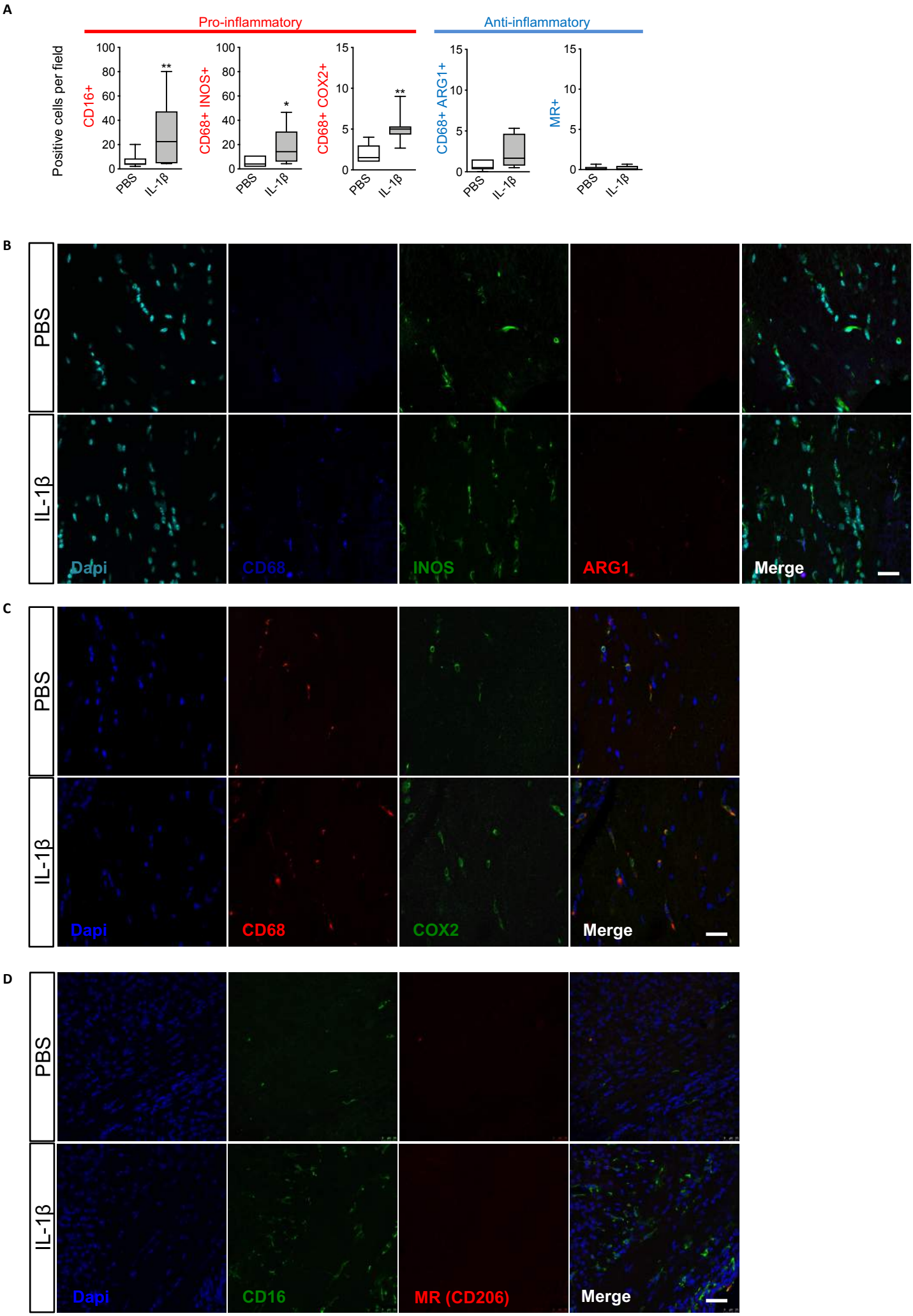
A
Pro-inflammatory
Anti-inflammatory
Positive cells per field
CD16+
CD68+ INOS+
CD68+ COX2+
CD68+ ARG1+
MR+
PBS
IL-1β
B
Dapi
CD68
INOS
ARG1
Merge
C
Dapi
CD68
COX2
Merge
D
Dapi
CD16
MR (CD206)
Merge

A

Properties	OG PBS	OG IL-1β	MG PBS	MG IL-1β
Nodes	571	1583	786	3113
Probes with description	505 (88%)	1411 (90%)	713 (90%)	2789 (90%)
Map to genes	243 (43%)	647 (41%)	469(57%)	1569 (50%)
Edges	1229	6457	1810	48104
Degree distbn power law exp	-1,647	-1,687	-1,719	-1,243
Power law R2	0,887	0,845	0,871	0,879
Clustering coefficient	0,27	0,313	0,251	0,475
Connected components	34	9	5	1
Network diameter	18	13	11	6
Network centralisation	0,058	0,035	0,049	0,082
Characteristic path length	5,5	4,2	4,7	2,9
Av no of neighbours	4,3	8,2	4,6	30
Network density	0,008	0,005	0,006	0,01

B

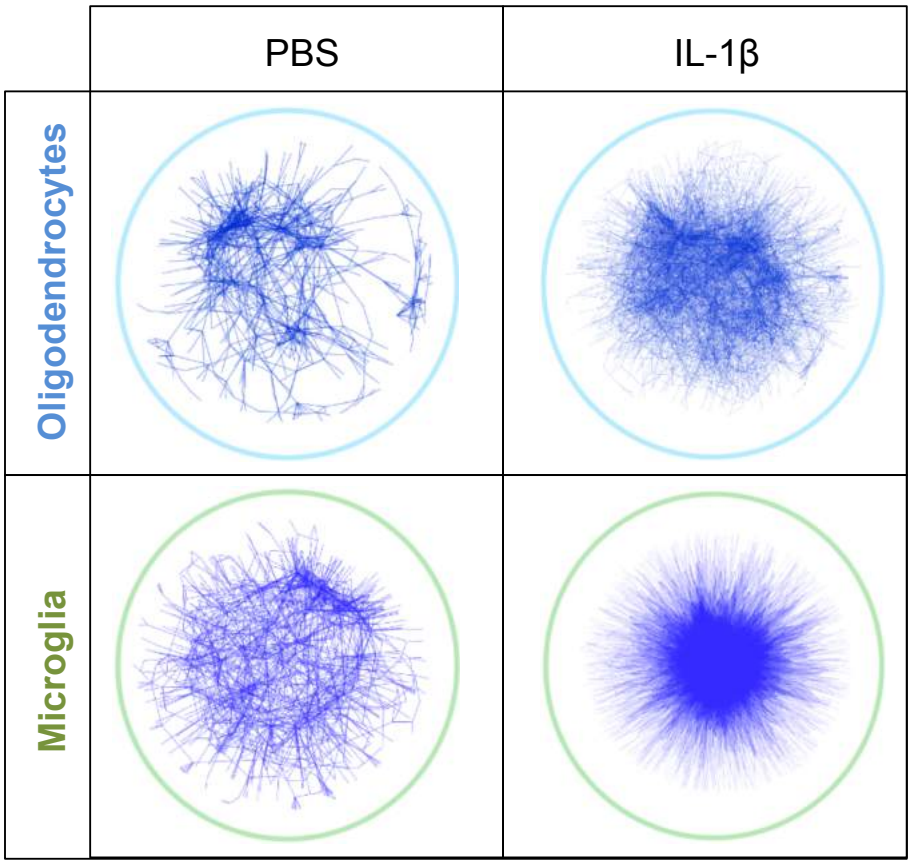

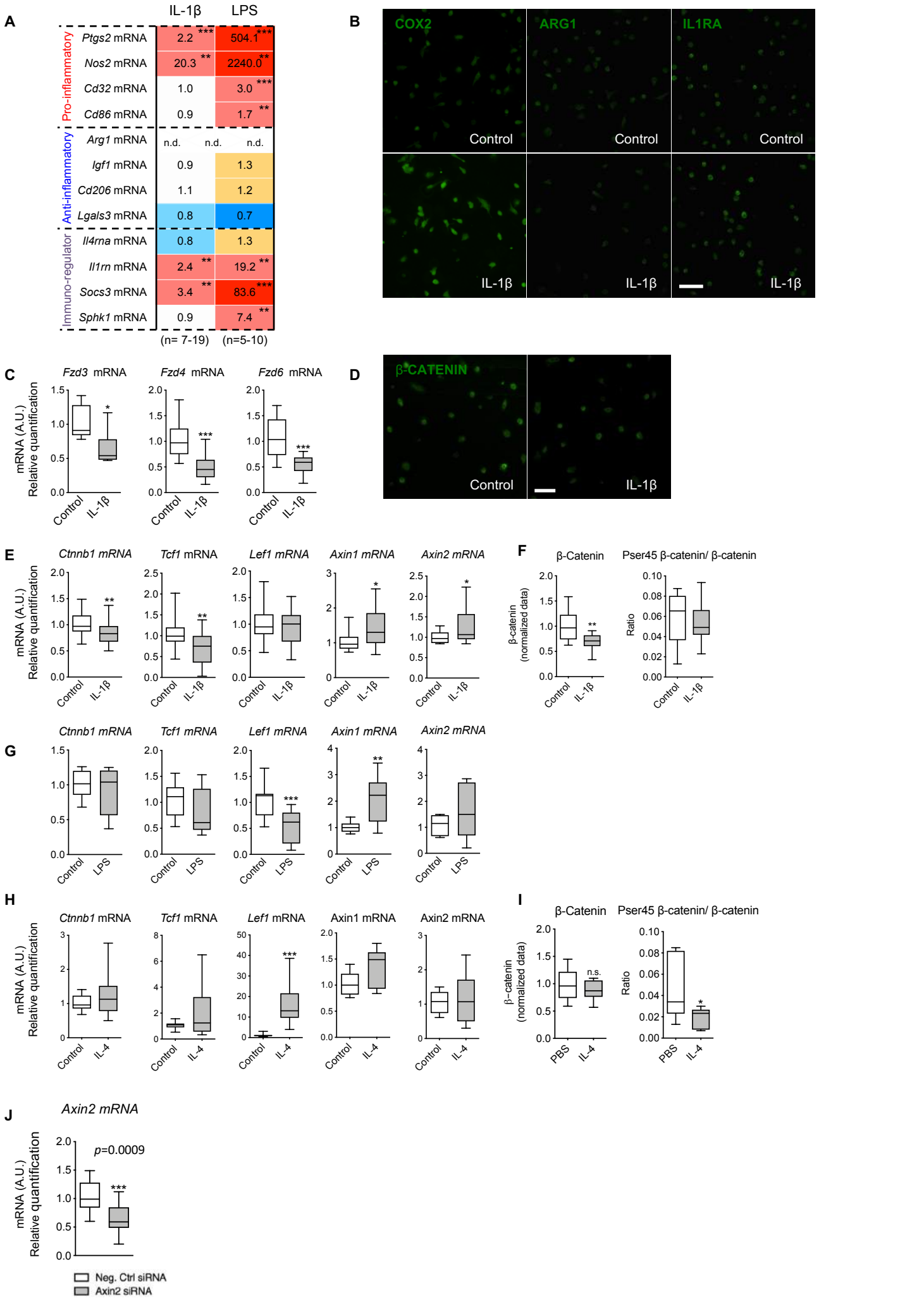
A
IL-1β
LPS
Pro-inflammatory
Anti-inflammatory
Immuno-regulator
Ptgs2 mRNA
Nos2 mRNA
Cd32 mRNA
Cd86 mRNA
Arg1 mRNA
Igf1 mRNA
Cd206 mRNA
Lgals3 mRNA
Il4rna mRNA
Il1rn mRNA
Socs3 mRNA
Sphk1 mRNA
2.2 ***
504.1 ***
20.3 **
2240.0 **
1.0
3.0 ***
0.9
1.7 **
n.d. n.d. n.d.
0.9
1.3
1.1
1.2
0.8
0.7
0.8
1.3
2.4 **
19.2 **
3.4 **
83.6 ***
0.9
7.4 **
(n= 7-19) (n=5-10)
B
COX2
ARG1
IL1RA
Control
IL-1β
C
Fzd3 mRNA
Fzd4 mRNA
Fzd6 mRNA
mRNA (A.U.)
Relative quantification
Control
IL-1β
D
β-CATENIN
E
Ctnnb1 mRNA
Tcf1 mRNA
Lef1 mRNA
Axin1 mRNA
Axin2 mRNA
F
β-Catenin
Pser45 β-catenin/ β-catenin
β-catenin (normalized data)
Ratio
G
LPS
H
IL-4
I
PBS
n.s.
J
p=0.0009
Neg. Ctrl siRNA
Axin2 siRNA

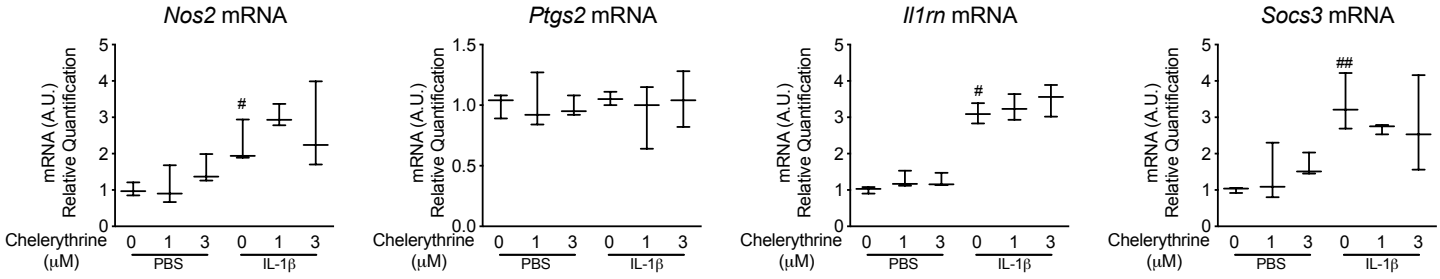
Nos2 mRNA
Ptgs2 mRNA
Il1rn mRNA
Socs3 mRNA
mRNA (A.U.)
Relative Quantification
Chelerythrine (μM)
0 1 3 0 1 3
PBS
IL-1β
#
##

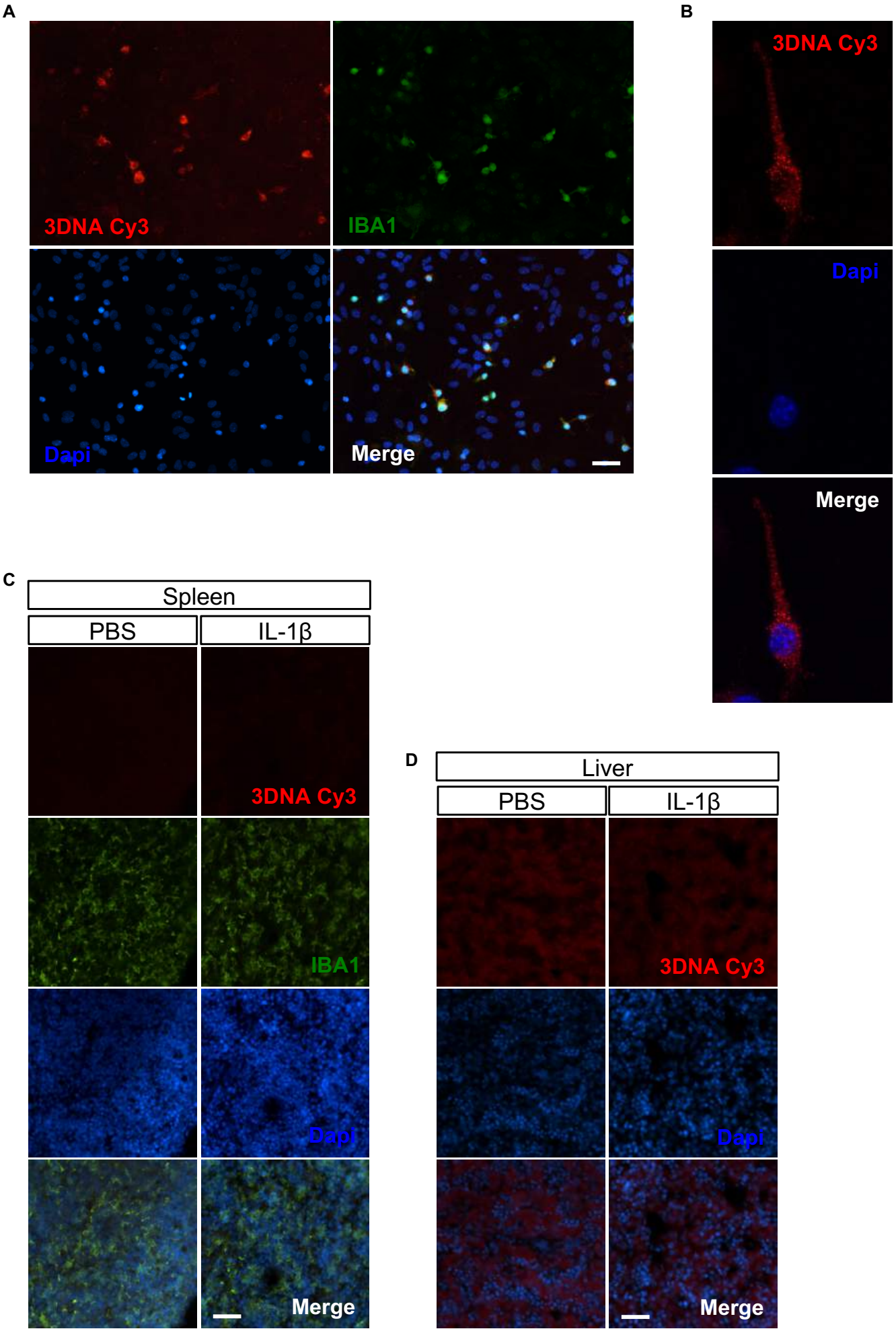
A
3DNA Cy3
IBA1
Dapi
Merge
B
3DNA Cy3
Dapi
Merge
C
Spleen
PBS
IL-1β
3DNA Cy3
IBA1
Dapi
Merge
D
Liver
PBS
IL-1β
3DNA Cy3
Dapi
Merge

A

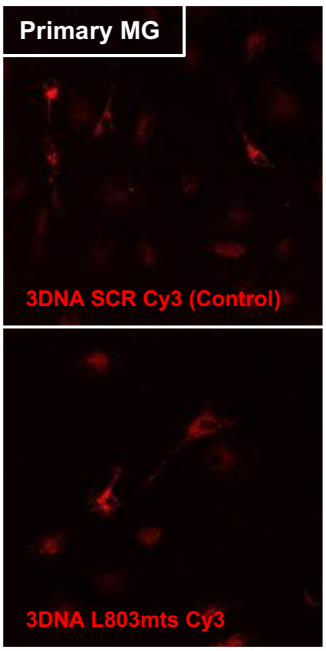
Primary MG
3DNA SCR Cy3 (Control)
3DNA L803mts Cy3

B

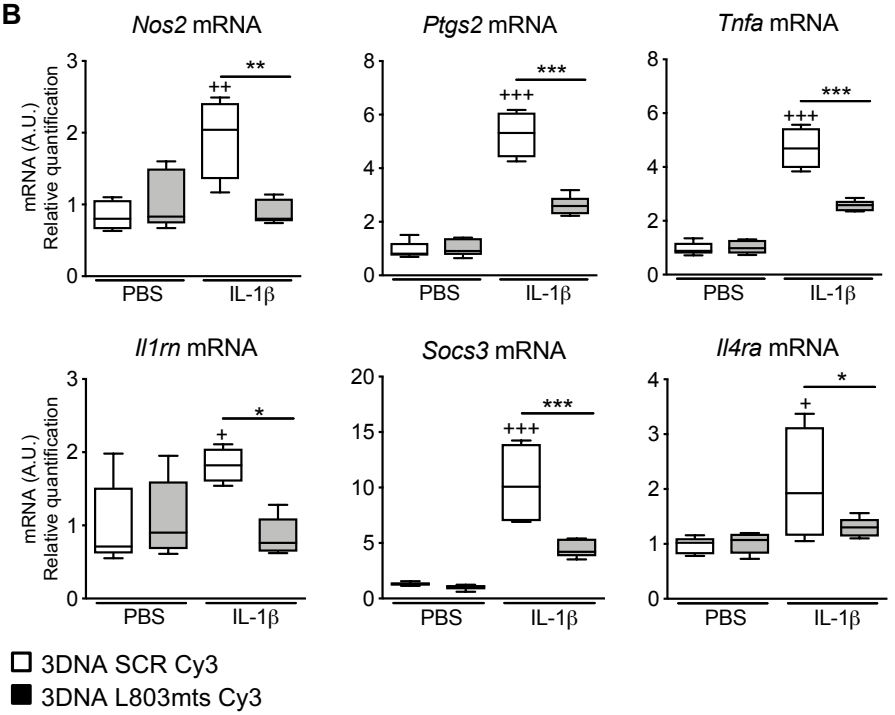
Nos2 mRNA
Ptgs2 mRNA
Tnfa mRNA
Il1rn mRNA
Socs3 mRNA
Il4ra mRNA
mRNA (A.U.)
Relative quantification
PBS
IL-1β
3DNA SCR Cy3
3DNA L803mts Cy3

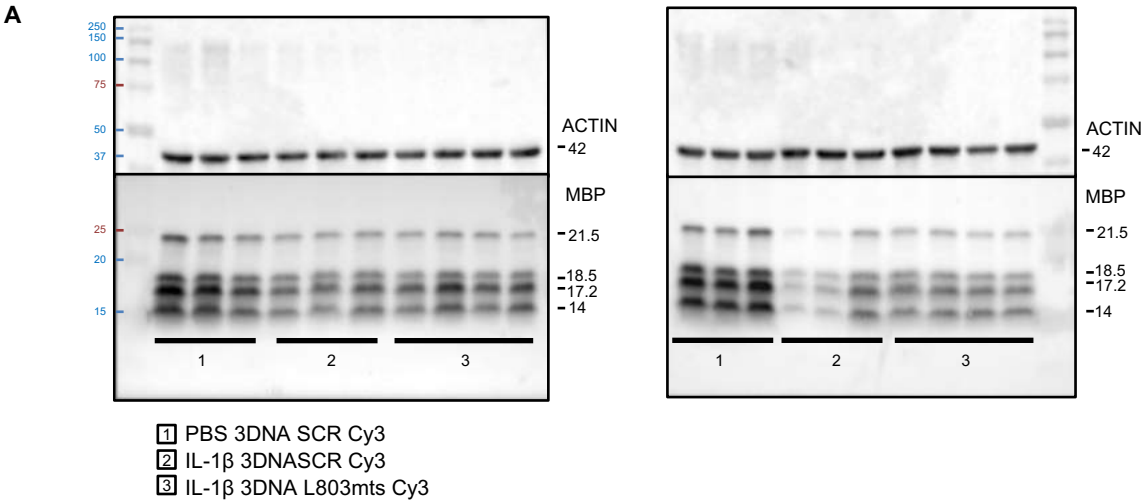
A
250
150
100
75
50
37
25
20
15
ACTIN
42
MBP
21.5
18.5
17.2
14
1
2
3
1 PBS 3DNA SCR Cy3
2 IL-1β 3DNASCR Cy3
3 IL-1β 3DNA L803mts Cy3

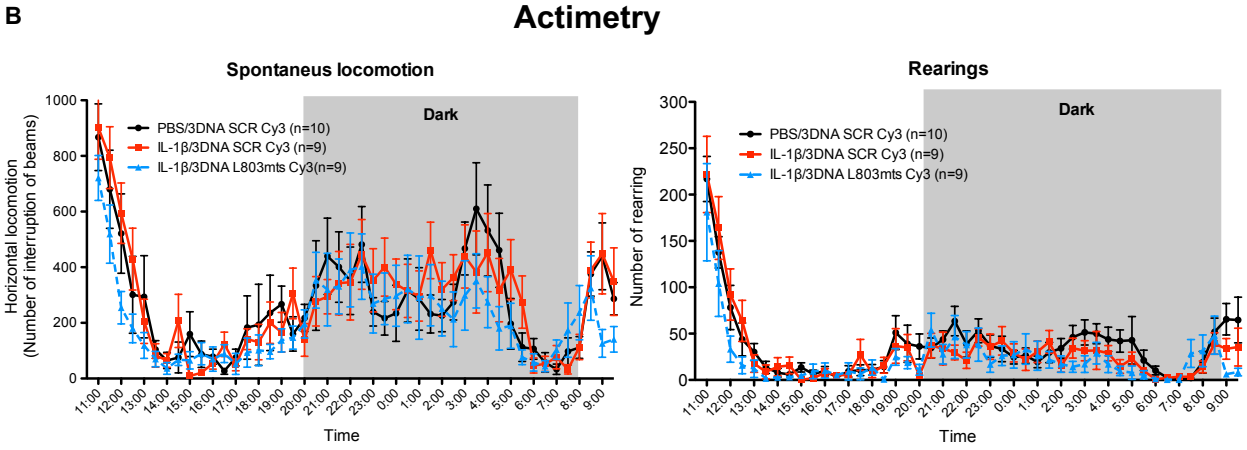
B
Actimetry
Spontaneus locomotion
Horizontal locomotion
(Number of interruption of beams)
PBS/3DNA SCR Cy3 (n=10)
IL-1β/3DNA SCR Cy3 (n=9)
IL-1β/3DNA L803mts Cy3(n=9)
Dark
Time
Rearings
Number of rearing
PBS/3DNA SCR Cy3 (n=10)
IL-1β/3DNA SCR Cy3 (n=9)
IL-1β/3DNA L803mts Cy3 (n=9)
Dark
Time

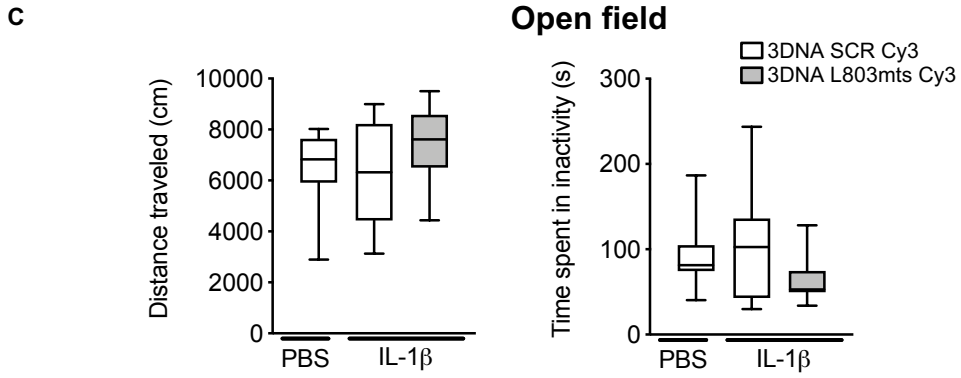
C
Open field
Distance traveled (cm)
10000
8000
6000
4000
2000
0
PBS
IL-1β
3DNA SCR Cy3
3DNA L803mts Cy3
Time spent in inactivity (s)
300
200
100
0
PBS
IL-1β